ELSEVIER

Molten salt self-cooled solid first wall and blanket design based on advanced ferritic steel

C.P.C. Wong[a,*], S. Malang[b], M. Sawan[c], I. Sviatoslavsky[c], E. Mogahed[c],
S. Smolentsev[d], S. Majumdar[e], B. Merrill[f], R. Mattas[e], M. Friend[a],
J. Bolin[a], S. Sharafat[d]

[a] *General Atomics, P.O. Box 85608, San Diego, CA 92186-5608, USA*
[b] *Fusion Nuclear Technology Consulting, Linkenheim, Germany*
[c] *University of Wisconsin, Madison, WI, USA*
[d] *University of California, Los Angeles, CA, USA*
[e] *Argonne National Laboratory, Argonne, IL, USA*
[f] *INEEL, Idaho Falls, ID, USA*

Available online 17 September 2004

Abstract

As an element in the U.S. Advanced Power Extraction (APEX) program, the solid first wall and blanket design team assessed innovative design configurations with the use of advanced nano-composite ferritic steel (AFS) as the structural material and FLiBe as the tritium breeder and coolant. The goal for the assessment is to search for designs that can have high volumetric power density and surface heat-flux handling capability, with assurance of fuel self-sufficiency, high thermal efficiency and passive safety for a tokamak power reactor. We selected the re-circulating flow configuration as our reference design. Based on the recommended material properties of AFS we found that the reference design can handle a maximum surface heat flux of $1 \, \text{MW/m}^2$, and a maximum neutron wall loading of $5.4 \, \text{MW/m}^2$, with a gross thermal efficiency of 47%, while meeting all the tritium breeding, structural design and passive safety requirements. This paper will cover the results of the following areas of assessment: material design properties, FW/blanket design configuration, materials compatibility, components fabrication, neutronics analysis, thermal-hydraulics analysis including MHD effects, structural analysis; molten salt and helium closed cycle power conversion system; and safety and waste disposal of the re-circulating coolant first wall and blanket design.
© 2004 Published by Elsevier B.V.

Keywords: Fusion; First wall; Blanket; Advanced ferritic steel; FLiBe; Re-circulation coolant; Systems study; Liquid metal MHD; Gas turbine

1. Introduction

In 1997 U.S. DOE initiated the Advanced Power Extraction (APEX) program. The goal for the program is to search for innovative first wall and blanket (FW/blanket) design solutions that would meet the

* Corresponding author. Tel.: +1 858 455 4258;
fax: +1 858 455 2838.
E-mail address: wongc@fusion.gat.com (C.P.C. Wong).

following APEX program design goals [1]:

- high volumetric power density and surface heat-flux handling capability;
- large design margins;
- assured fuel self-sufficiency;
- low failure rates;
- high thermal efficiency;
- passive safety.

One element of the APEX program is the solid FW/blanket design assessment. In 1999, the solid FW assessment team completed a W–Re alloy, helium-cooled, lithium breeder, FW/blanket design with a 57.5% thermal efficiency [2]. In FY00 the team completed the development and assessment of a practical design for the high-temperature refractory solid FW/blanket option, with focus on the vaporized lithium EVOLVE concept [3,4], and identified the need to address the issue of MHD effects on the boiling of liquid metal. Subsequently, experiments to address the MHD effect on the boiling of lithium were performed at the University of Wisconsin and results showed that the MHD effects are manageable as projected [5]. We also identified the concern on the fabrication of FW/blanket components using W–Re alloy. In 2001, we completed the evaluation of the low activation SiC/SiC LiPb cooled FW/blanket concept and confirmed the need to further quantify the radiation damage of SiC/SiC composite and the compatibility between SiC and LiPb. In 2002, the solid FW assessment team initiated the evaluation of concepts using advanced nano-composite ferritic steel (AFS) as the structural material and FLiBe as the tritium breeder and coolant. Design limits of this combination of materials were selected, and after an evaluation of different proposed FW/blanket configurations, the re-circulating flow configuration was selected as the reference design for more detailed evaluation. In 2003 we completed the evaluation of the AFS/FLiBe FW/blanket concept. This paper presents the overview of this design. The areas of design development, neutronics analysis, thermal-hydraulics and structural analyses; and the power conversion system are presented in this paper. Reference [6] covers in more detail the areas of FW/blanket geometry, materials, materials compatibility, structural evaluation, fabrication and fluid circuits. Reference [7] covers details on the assessment of the safety design of this re-circulating coolant AFS/FLiBe FW/blanket concept.

2. Selected materials

For our design we selected FLiBe as the coolant and tritium breeding material, Pb as the neutron multiplier and AFS as the structural material. This section describes the characteristics and interaction between these materials.

2.1. Breeder material

The selected coolant material is FLiBe. It has been proposed for use as self-cooled tritium breeding material for both magnetic and inertial confinement fusion reactors [8,9], because it has acceptable heat transfer properties, low electrical conductivity leading to small MHD effects, and is relatively inert to air or water compared to liquid metals. Two compositions of the molten salt have been proposed, one ($LiF_2 \cdot BeF_2$), which has a lower viscosity and a high melting temperature ($459\,°C$) and the other ($LiF_{0.88} \cdot BeF_2$) has a higher viscosity and a lower melting temperature ($363\,°C$). The lower viscosity composition has been chosen, in spite of the higher melting temperature. The use of FLiBe as breeder and coolant enables simple self-cooled blanket designs without the need for electrical insulators between coolant and walls since the electrical conductivity of this molten salt is orders of magnitudes lower than that of lead–lithium or lithium. However, there are a number of obstacles making the design of FLiBe-blankets a challenging task.

Main issues include:

(a) The thermal conductivity of FLiBe is exceptional low ($1\,W/m\,K$) compared to $15\,W/m\,K$ for Pb–17Li and $50\,W/m\,K$ for Li. To obtain sufficiently large heat transfer, high turbulence flow is required.

(b) The viscosity of FLiBe is really high, especially at temperatures close to the melting point. At a temperature of $500\,°C$ for example, the kinematic viscosity is $11.5 \times 10^{-6}\,m^2/s$ compared to $0.12 \times 10^{-6}\,m^2/s$ for water at $300\,°C$, $15\,MPa$ (PWR-conditions). This means that high velocities and/or large channel dimensions are required to obtain sufficient turbulence.

(c) The tritium breeding capabilities of FLiBe are relatively limited, making the use of an additional neutron multiplier mandatory. Candidate materi-

als for neutron multipliers are either beryllium or lead. Usually a region of beryllium with a thickness of 3–5 cm is arranged close to the FW, either as porous plates or pebble beds. This implies the problem of beryllium swelling under neutron irradiation (10–15 vol.% at the end-of-life conditions), and a large tritium inventory in the beryllium (up to some kilograms), which is a safety concern. If lead is selected, about the same thickness of the multiplier region close to the FW is required to achieve tritium self-sufficiency. This results in lower energy multiplication, more severe compatibility problems with the structural material compared to beryllium, and requires online purification to avoid excessive build-up of the alpha-emitter polonium. However, it avoids the problems associated with high tritium inventory and swelling which are probably inherent problems for beryllium. We considered these trade offs and selected lead as the neutron multiplier for our evaluation.

(d) The high melting point of FLiBe (459 °C for $(LiF)_2(BeF_2)$) requires a structural material with a temperature range up to >650 °C. In addition, FLiBe is rather aggressive to a number of candidate structural materials, with the formation of hydrogen fluoride (HF). To limit the formation of HF, one approach is the REDOX control. This requires an excess of beryllium in contact with the FLiBe to encourage the formation of BeF. This contact can be provided either inside the blanket or outside the irradiation environment [6]. The rather low upper temperature range of classical steels was for a long time the main reason not to consider FLiBe as a viable breeder material. However, AFS alloys have the promise of sufficient strength up to 800 °C, and allowable interface temperatures at the FLiBe/steel interface up to 700 °C [6]. This large temperature window is the main reason why the combination of FLiBe and AFS steel has been chosen for our design.

2.2. Neutron multiplier

From a nuclear performance point of view, beryllium is the best neutron multiplier, characterized by small neutron absorption and a low energy threshold for (n, 2n) reactions. However, as presented above, to avoid the problems associated with high tritium inventory and swelling, which are probably inherent problems for beryllium, we considered lead as the alternate neutron multiplier. However, the effectiveness of lead as a neutron multiplier decreases with increasing distance from the FW, since the neutron energy drops relatively fast below the (n, 2n) threshold for neutron multiplication. Another problem encountered with the use of lead is caused by the melting point of 327 °C. In general, this temperature is too low to keep the multiplier solid and usually too high to maintain it liquid under all operational conditions. However, in connection with a melting point of 459 °C for the FLiBe breeder, and the high temperature limits of the anticipated AFS, lead becomes more feasible for this blanket concept. Furthermore, in an FLiBe blanket a relatively thin multiplier layer behind the first wall is sufficient for achieving tritium self-sufficiency. Initial scoping calculations indicated that either 2.5 cm of solid beryllium or 4 cm of lead are required. These are additional reasons why lead is selected as the multiplier material for the proposed blanket concept. An issue to be observed with lead is the high volumetric heat generation. A peak value of 38 W/cm^3 for a neutron wall load of 5 MW/m^2 has been determined. This means that the lead located close to the first wall has to be intensively cooled.

2.3. Structural material

To improve the acceptability of fusion energy for producing electricity, scientists and engineers have been evaluating different structural materials, coolants, breeders and neutron multipliers. Ferritic steels have always been attractive, since they are known to experience low swelling due to irradiation and can be formulated to be low activation. However, their use has been limited to rather low temperature, the order of 550 °C, limiting the coolant temperature, and consequently, the power cycle efficiency. Several years ago, metallurgists began experimenting with mixing ferritic steel with minute amounts of ceramic materials to improve high temperature strength. One formulation that is being developed at ORNL (designated 12YWT) [10–12] has 0.25% of yttria mixed in. This ODS ferritic steel alloy appears to have superior properties and opens up new possibilities for higher coolant temperatures and improved power cycles. It appears to

have a maximum working temperature of 800 °C and a corresponding yield strength of 320 MPa. When used with the molten salt coolant FLiBe, the recommended maximum allowable temperature is 700 °C [6] as noted above.

Another material design issue arose when molten lead was proposed as a multiplier instead of Be. The issue was the maximum allowable interface temperature between molten Pb and AFS. A relatively high temperature of 700 °C was shown to be acceptable from static tests, but with close control of the oxygen [6]. For this study we have selected this as maximum allowable interface temperature between the Pb and the steel, which will have to be further confirmed by experiment. Furthermore, as an alternative, to obtain such a high allowable interface temperature a thin coating ($\sim$10 µm) of W or Ta could be applied to the inside surface of the tubes containing Pb. This can be done with plating or by plasma deposition. A detailed presentation on the properties of AFS and the issue of materials compatibility are given in reference [6].

3. Configuration

For the selection of FW/blanket configuration, there are mainly two conflicting requirements to be resolved for a self-cooled FLiBe blanket:

1. Sufficient cooling of the FW and multiplier region requires high coolant velocities and high turbulence in this region to overcome the impact of low thermal conductivity and high viscosity of FLiBe. This requires, for reasonably low-pressure drops, rather large coolant channels and high mass flow rates, which results in a low temperature rise in the FW region.
2. Efficient power conversion systems require a high coolant exit temperature in the blanket and a reasonably large temperature rise between blanket inlet and exit. This limits the mass flow rate to the power conversion system and results usually in high maximum structural temperatures and high temperatures at the structure/coolant interface.

After studying several different blanket geometries and flow schemes, we selected a concept with the following main characteristics.

3.1. Thermal insulation between structures and coolant

Self-cooled blankets have the potential to achieve coolant exit temperatures higher than the maximum interface temperature and in some cases higher than the maximum structure temperature. This has been demonstrated with the ARIES-ST [13] and ARIES-AT [14] blanket concepts where the volumetric heating of the liquid breeder results in exit temperatures 100–150 K higher than the maximum structure temperature. The key feature of such concepts is to cool the structure with the "cold" inlet flow, and to limit heat losses from the "hot" zones to the structure by employing an additional insulator (ARIES-ST) or by low heat transfer coefficients (ARIES-AT). In the proposed FLiBe blanket concept the same principle is employed as in ARIES-AT. This means the coolant is routed first through channels in the structure including the FW before it is heated up further by volumetric heating in large exit channels, flowing there with low velocity.

3.2. Recirculation of first wall coolant

An attractive blanket should allow for surface heat fluxes of 0.5 MW/m^2 or more. Usually steel first walls are limited to about 1 MW/m^2 from heat transfer consideration. This implies that the heat transfer coefficient in the FW cooling channels should be at least 10,000 W/m^2 K. What does this mean for FLiBe as a coolant? If for example the bulk temperature is 500 °C and the channel hydraulic diameter 0.01 m, the required re-number is 6100 and the coolant velocity about 7 m/s. This would result in a pressure drop rate of about 0.18 MPa/m, a rather high value for an 8 m high blanket segment. Furthermore, if a once-through flow scheme were chosen, the resulting temperature rise would be rather small. This example indicates that for efficient FW cooling the desirable parameters are large diameter, high velocity and high bulk temperature. All three design goals can be reached if the coolant flow rate in the FW channels is made considerably higher than the flow rate to the power conversion system, which can be achieved by employing a bypass to the flow in the large central channel leaving the blanket segments. Such a flow scheme is shown in Fig. 1. In this figure a pump is arranged at the in-
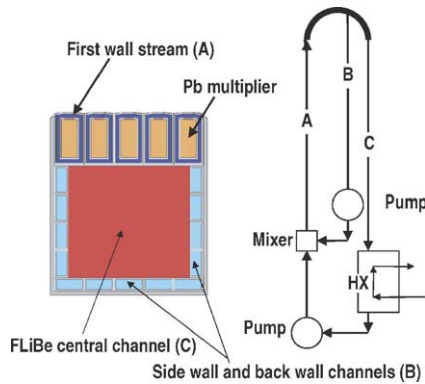
Fig. 1. FW/blanket cross-section and coolant routing.

Table 1
Radial build of the reference re-circulating flow blanket

Zone	Thickness (mm)	Volume fraction		
		FLiBe	AFS	Pb
1. First wall	3		1	
2. FW FLiBe channel, poloidal flow	10	0.92	0.08	
3. Pb front wall	3	0.2333	0.7667	
4. Pb mulitplier	40	0.2333	0.18	0.5867
5. Pb back wall	3	0.2333	0.7667	
6. FLiBe channel + side wall	7	0.92	0.08	
7. FLiBe channel back wall	6		1	
8. FLiBe + side walls, a mixed zone	199	0.932	0.068	
9. Back wall, a mixed zone	29	0.6069	0.3931	
Total	300			

let to the blanket, pushing the coolant stream A from the bottom through the FW/multiplier region. At the top of the blanket the coolant stream is divided into a bypass stream B and an exit stream C, flowing to the heat exchanger of the power conversion system. There is a second pump arranged controlling the split between exit flow C and bypass flow B. Both coolant streams are mixed after the heat exchanger (HX), and the coolant temperature at the blanket exit as well as the one at the blanket inlet depend on the mixing ratio. Interesting results of this flow scheme are a blanket inlet temperature considerably higher than the minimum FLiBe temperature after the HX, and a higher ratio between heat transfer coefficient and pressure drop in the FW cooling channels compared to a once-through flow scheme. Fig. 1 also shows a simplified cross section of a blanket element, neglecting the trapeze-shape of real blanket elements, and the use of multiple elements to form a blanket sector. Presented is an element cross-section of 0.3 m in toroidal direction and 0.3 m in radial direction. This radial thickness is sufficient to make the next blanket zone to be a lifetime component. There are rectangular tubes filled with stagnant, or slowly circulating, lead arranged behind the FW cooling channels. FLiBe coolant channels, providing sufficient cooling of the FW and multiplier, surround these tubes. The large central channel behind FW/multiplier region is enclosed by cooling panels, providing the cross section for the bypass stream, and serving at the same time as a cooled liner for the central channel.

4. Neutronics analysis

Neutronics calculations were performed to determine the relevant nuclear performance parameters for the blanket with lead multiplier. These include tritium breeding, nuclear heating, radiation damage, and shielding requirements. In addition, the design option with beryllium multiplier was analyzed and compared to the reference design. Table 1 gives the radial build used in the calculations. The material composition of each zone is listed. In the outboard (OB) side, the re-circulating blanket is followed by a 40 cm thick secondary blanket consisting of 94% FLiBe and 6% AFS structure. Due to limited space, no secondary blanket is utilized in the inboard (IB) region. The ONEDANT module of the DANTSYS 3.0 discrete ordinates particle transport code system [15] was used to perform the calculations utilizing the FENDL-2 [16] nuclear data library. Both the IB and OB regions were modeled simultaneously to account for the toroidal effects. The results were normalized to the peak neutron wall loading values of 5.45 and 3.61 MW/m^2 in the OB and IB regions, respectively. The results of the neutronics calculations are summarized here.
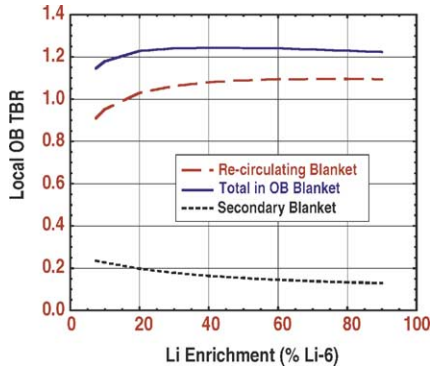
Fig. 2. Local TBR in OB region with re-circulating flow blanket.

Fig. 3. Radial distribution of power density in blanket components.

4.1. Tritium breeding

Fig. 2 shows the effect of enriching Li in 6Li on the local OB tritium breeding ratio (TBR). The contributions from the re-circulating and secondary blankets are shown separately. Since the TBR has a flat peak in the enrichment range between 40 and 60%, an enrichment of 40% [6]Li is chosen. At this enrichment the secondary blanket contributes ~13% of the local OB TBR of 1.244. The results also indicated that the TBR is not very sensitive to the Pb zone thickness. Only ~3% enhancement in the TBR is achieved by increasing the Pb zone thickness from 4 to 8 cm. Assuming neutron coverage of 75% for the OB region, 15% for the IB region, and 10% for the divertor region, the overall TBR will be ~1.11 excluding breeding in the divertor region. Breeding in the divertor zone could add ~0.05 depending on the amount of FLiBe used. Hence, we expect that tritium self-sufficiency can be realized in a fusion power plant employing the re-circulating flow blanket.

4.2. Nuclear heating

The total nuclear energy multiplication in the 30 cm thick re-circulating IB and OB blankets and 40 cm thick OB secondary blanket is 1.13. The OB secondary blanket contributes 4.5% of the total IB and OB nuclear heating. This corresponds to only ~3.7% of the total IB and OB thermal power that includes surface heating. Nuclear heating radial profiles in the different blanket components were determined for use in the thermal-

hydraulics analysis. The results are shown in Fig. 3 for a unit neutron wall loading. The poloidal distribution of neutron wall loading can be used to determine the nuclear heating at the different poloidal locations. The total power generated from nuclear heating was calculated for the different zones of the re-circulating blanket module using the average OB and IB neutron wall loading values of 4.6 and 2.8 MW/m^2, respectively, and a module height of 8 m. The results for the OB and IB modules are given in Table 2. The surface heat flux adds 2.14 and 1.92 MW to the thermal power in the OB and IB first wall zones, respectively.

4.3. Radiation damage

The peak radiation damage parameters in the AFS structure were calculated. The peak OB dpa and helium production rates are 77.6 dpa/FPY and 955 He appm/FPY. The corresponding values for the IB mod-

Table 2
Power from nuclear heating in the zones of the blanket module

Zone	Power from nuclear heating (MW)	
	OB module	IB module
First wall	4.86	2.96
Side wall	1.14	0.69
Back wall	0.31	0.19
Central FLiBe channel	4.88	2.97
Total	11.19	6.81
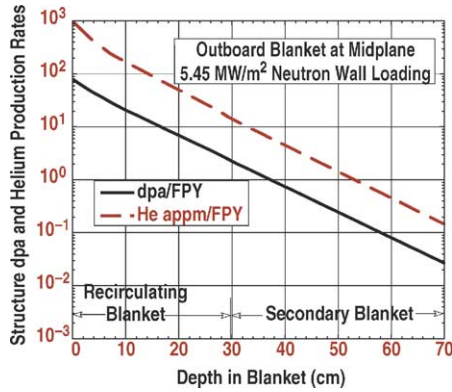
Fig. 4. Radial variation of structure damage at OB midplane.

ules are 61.7 dpa/FPY and 719 He appm/FPY. Based on a radiation damage limit of 200 dpa, the lifetime of the re-circulating blanket is expected to be ∼3 FPY. The peak cumulative end-of-life (30 FPY) dpa in the AFS structure of the OB secondary blanket is 60.3 dpa implying that it will be a lifetime component. Fig. 4 shows the radial profile of the radiation damage in the structure of the re-circulating and secondary blankets at the OB midplane.

4.4. Shielding requirement

Calculations were performed to determine the radial build in both the IB and OB regions required to provide adequate shielding for the vacuum vessel (VV) and TF magnet coils. Table 3 lists the required radial build. This results in all VV and magnet radiation limits being satisfied. The peak end-of-life helium production in the VV is 0.4 appm allowing for rewelding. The peak values of end-of-life fast neutron fluence and insulator dose in the magnet are 2.4×10^{18} n/cm^2 and $4.4 \times$

Table 3
Radial build required for adequate shielding

Zone	Outboard (cm)	Inboard (cm)
Re-circulating blanket	30	30
Secondary blanket	40	0
Shield	10	40
Vacuum vessel	30	30
TF magnet	60	60

10^9 rad which are below the widely accepted limits of 10^{19} n/cm^2 for Nb$_3$Sn and 10^{10} rad for polyimides.

4.5. Impact of using Be instead of Pb

The option of replacing the liquid lead multiplier in the re-circulating blanket by beryllium pebbles was considered. The radial build is similar to that given in Table 1 with the exception that the thickness of the multiplier region (zone 4) is reduced to 37 mm with 32.2% FLiBe, 8% NCF, and 59.8% Be. Zones 3 and 5 include 100% NCF and the thickness of zone 6 is increased to 10 mm. The neutronics calculations with this radial build yield a local OB TBR of 1.322 out of which ∼10% is contributed by the 40 cm thick secondary blanket. Excluding breeding in the divertor region, the overall TBR is estimated to be ∼1.17. This is ∼6% larger than that for the reference design with Pb multiplier. The total nuclear energy multiplication in the IB and OB 30 cm re-circulating blankets and OB secondary blanket is 1.24 compared to 1.13 with Pb. Total nuclear heating in the re-circulating blanket is ∼10% higher than in the case with Pb multiplier. The increase in heating occurs primarily in the front zone of the blanket. Nuclear heating in the first wall zone increases by ∼28%. A critical issue associated with using Be in fusion blankets is the amount of tritium produced and retained in the beryllium. The total amount of tritium produced in the Be pebbles used in all IB and OB modules is 2.4 kg at end-of-life of the blanket (3 FPY). The tritium inventory will be much lower than the tritium production due to tritium permeation out of Be at the high Be temperatures.

4.6. Radioactivity, decay heat, and radwaste for the reference blanket

Activation calculations were performed for the reference re-circulating blanket with Pb multiplier to determine the generated radioactive inventory and decay heat. Detailed results were used for safety assessment and are given in reference [7]. Fig. 5 shows the total activity generated in the blanket constituents as a function of time following shutdown. Fig. 6 gives the decay heat results. It is clear that the AFS structure dominates the total activity and decay heat. The radwaste of the different components of the blanket were evaluated. The Mo
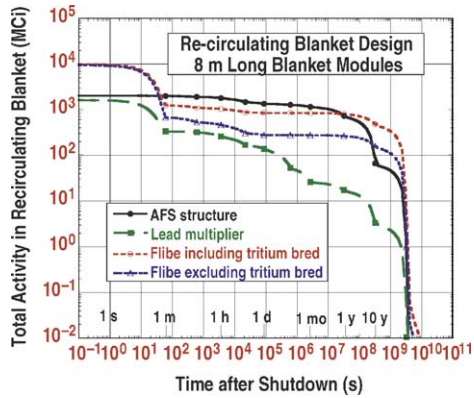
Fig. 5. Total activity in the blanket constituents.
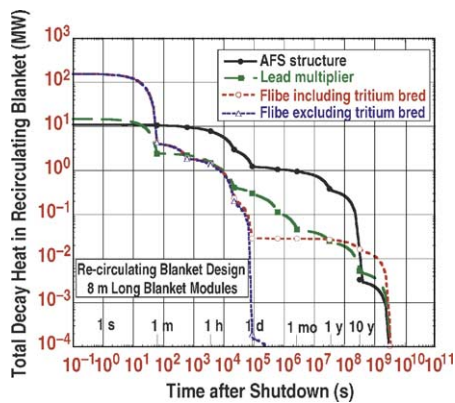
Fig. 6. Total decay heat in the blanket constituents.

content in the AFS needs to be reduced from 0.02% to <0.01% for the structure waste to qualify as low level class C waste. In addition, an attempt should be made to eliminate or limit concentration of impurities such as Nb and Ag to less than about 1 wppm. While the waste disposal rating (WDR) of the FLiBe is well below unity, the WDR for stagnant Pb is ~50 implying that it has to be circulated at a very small velocity (<10^{-5} m/s) to remove the generated ^{208}Bi through possibly diffusion type cold traps [17], and allow Pb disposal as low level waste [7].

5. Parametric thermal-hydraulics design and systems assessment

A thermal-hydraulics design evaluation was performed to search for the reference AFS/FLiBe

Table 4
Material temperature limits for the reference design

Maximum temperature limit for AFS (°C)	800
Maximum temperature limit for AFS/FLiBe interface (°C)	700
Maximum temperature limit for AFS/Pb interface (°C)	700

FW/blanket design. This consists of a systems study to determine the reactor embodiment of the blanket module and the corresponding neutron and surface heat flux wall loadings. To select the reference design, iterations between systems, neutronics and thermal-hydraulics analysis were performed as determined by temperature limits of selected materials. After the reference design was selected, a more detailed thermal-hydraulics design assessment, including MHD effects to the FLiBe coolant, was performed and corresponding results are presented in the next section.

5.1. Thermal-hydraulics design temperature limits

The key design temperature limitations for the combined use of AFS as structural material, FLiBe as the tritium breeder and coolant, and Pb as the neutron multiplier are given in Table 4 [6].

These temperature design limits together with the selected FW/blanket module configuration were then used to determine the thermal-hydraulics parameters of the design.

5.2. Module configuration

The inboard and outboard FW/blanket modules of a tokamak reactor are shown in Fig. 7. With the selected flow configuration, the flow parameters of the first wall, side wall and central channel coolant streams can be adjusted by changing the mass flow rate of the re-circulating stream (stream B of Fig. 1), which is controlled by the re-circulating pump located at the bottom of the module as shown. But the exact location of the re-circulating pump in the tokamak has not been defined. For a 16 toroidal field coils and 16 sectors tokamak reactor design, there are 5 poloidal inboard modules and 9 poloidal outboard modules per sector. The inboard and outboard modules at the midplane have similar width of 0.3 m. Hydraulic dimensions of these modules are also similar. It should be noted that for the

Table 5
Thermal-hydraulics parameters of the inboard and outboard FW/blanket modules

	Inboard	Outboard
Number of module per sector	5	9
Midplane module width (m)	0.3	0.3
Input power per module		
Module power (MW)	8.7	13.2
First wall including heat flux (MW)	5.8	6.9
Side + back wall (MW)	0.88	1.45
Central FLiBe column (MW)	2.97	4.88
First wall and Pb zone at inlet/midplane/outlet, of the outboard, unless specified		
FW heat flux (MW/m^2)	0.73/0.86/0.73	0.73/1/0.73
Maximum neutron wall loading (MW/m^2)	1.9/3.6/1.9	2.8/5.4/2.8
Neutron poloidal peaking factor to chamber average	0.95	1.42
FW mass flow rate (kg/s)	71.2	98.6
$T_{coolant}$-bulk (°C)	585/602/619	585/599/614
FLiBe velocity (m/s)	4.57/4.59/4.61	6.33/6.36/6.38
Hydraulic diameter (cm)	1.54	1.54
Re	11012/12230/13529	15259/16698/18218
h (W/m^2 K)	9264/9866/10482	12427/13118/13821
FW AFS/FLiBe $T_{interface}$ (°C)	669/699/694	650/687/673
FW T_{max} (°C)	738/791/763	720/799/743
Pressure drop (MPa)	0.41	0.74
Midplane Pb wall AFS/FLiBe interface T (°C)	625	633
Midplane Pb wall AFS/Pb interface T (°C)	649	679
Midplane Pb max (°C)	922	1186
Side and back wall at inlet/midplane/outlet, unless specified		
Mass flow rate (kg/s)	51	68
$T_{coolant}$-bulk (°C)	619/623/626	614/619/623
Midplane FLiBe velocity (m/s)	2.75	2.75
Hydraulic diameter (cm)	2.61	2.61
Midplane Re	10262	13360
Midplane h (W/m^2 K)	4796	6125
Pressure drop (MPa)	0.050	0.084
Central FLiBe zone at inlet/midplane/outlet unless specified		
Mass flow rate (kg/s)	20.17	30.6
$T_{coolant}$-bulk (°C)	619/650/681	614/649 /681
Midplane FLiBe velocity (m/s)	0.22	0.33
Estimated residence time (s)	36	24
Hydraulic diameter (cm)	21.8	21.8
Midplane Re	10490	15734
Midplane h (W/m^2 K)	558	807
Pressure drop (MPa)	0.000066	0.000137
Total module FW/blanket pressure drop (MPa)	0.464	0.820

following thermal-hydraulics analysis, uniform flow cross-section of the FW/blanket module was assumed. For the reactor outboard there are front and secondary blankets. The secondary blanket will pick up 3.7% of the total reactor thermal power.

5.3. Thermal-hydraulics parametric assessment and results

For the thermal-hydraulics parametric assessment, the following inputs and assumptions were used:

Table 6
Parameters of the recirculating blanket tokamak reactor design based on systems evaluation

	Task IV tokamak reactor
R_0 (m)	5.4
Elongation	2.2
Aspect ratio	3.6
Blanket height (m)	7.82
B_0 (T)	5.77
I_p (MA)	16.9
Bootstrap fraction (%)	90
Z_{eff}[a]	1.876
Rad fraction	0.676
Maximum FW ϕ (MW/m^2)	1
Ave NWL (MW/m^2)	3.8
Blanket (M)	1.15
P_α (MW)	550
P_{fusion} (MW)	2755
$P_{e\text{-}gross}$ (MW)	1514
$P_{e\text{-}net}$ (MW)	1289
η_{th} (%)	47
P_{brem} (MW)	60.8
P_{ow}-impurity radiation (MW)	362
P-CD (MW)	74
β_N	5.7
β_t (%)	11.1
β_p (%)	2.13

[a] Plasma core impurities content: He^3: 0.00074, He^4: 0.22243, O$_2$: 0.005, Fe: 0.0008.

1. Radial distributions of power density for the first wall, sidewalls, backwall, neutron multiplier and the FLiBe zones were obtained from neutronics calculations, presented in the previous section.
2. Inboard and outboard FW/blanket designs were considered. Since the outboard secondary blanket intercepts only 3.7% of the total reactor thermal power, only the front outboard blanket design was considered in this analysis.
3. To get the polodial distribution of surface heat flux, 14% of the plasma core radiation is from Bremsstrahlung radiation and it has a poloidal power distribution. The remaining 86% is from line-radiation, which is distributed uniformly to the reactor chamber.

Fig. 8 shows the parametric results of the thermal-hydraulics analysis for the outboard FW/blanket design, including the first wall maximum temperature located at the outboard midplane, interface temperature between AFS and FLiBe and interface temperature between AFS and Pb; and the corresponding total

module pressure drop as a function of re-circulating stream mass flow rate. These results were generated with an average and maximum neutron wall loading of 3.8 and 5.4 MW/m^2, respectively, a maximum surface heat flux at the outboard midplane of 1 MW/m^2; and a coolant inlet and outlet temperature of 500 and 681 °C, respectively. Results show that the first wall maximum temperature limits the design. When the first wall is designed to the maximum allowable first wall temperature of 800 °C, both the AFS/FLiBe and AFS/Pb interface temperatures can be kept below 700 °C. Fig. 8 also shows that lower material temperatures can be obtained at the expense of higher coolant pressure-drop, which will have direct impact on the mechanical stresses of the module. As an example with a 25 °C reduction in the allowable first wall maximum temperature, the total FW/blanket pressure drop would be increased by more than a factor of 2 from 0.8 to 1.75 MPa. Similarly, a reduction in the allowable interface temperature between Pb and AFS by 25 °C, the total FW/blanket pressure drop would be increased also by more than a factor of 2 as shown in Fig. 8.

Fig. 9 shows additional outboard blanket design parametric results: first wall mass flow rate, neutron wall loading, surface heat flux, total system pressure drop and corresponding molten salt closed gas cycle (MCGC) gross thermal efficiency, as a function of coolant outlet temperature. These results were calculated with a coolant inlet temperature of 500 °C and a maximum AFS temperature of <800 °C. Results show that with the selected configuration and coolant routing scheme, designs with higher surface loading >1 MW/m^2 and correspondingly average neutron wall loading >3.8 MW/m^2 are possible, but with penalties of higher system pressure drop, lower coolant outlet temperature and with correspondingly lower gross thermal efficiency.

Based on the parametric results shown in Figs. 8 and 9 we selected our reference design point and key thermal-hydraulics parameters for the outboard FW/blanket module design as given in Table 5. Similar assessment was performed for the inboard FW/blanket module design and corresponding parameters are also presented in Table 5.

We found that by adjusting the re-circulation flow mass flow rate, the inboard temperatures can be adjusted to be similar to the outboard blanket temperatures, even though the outboard blanket is limited by
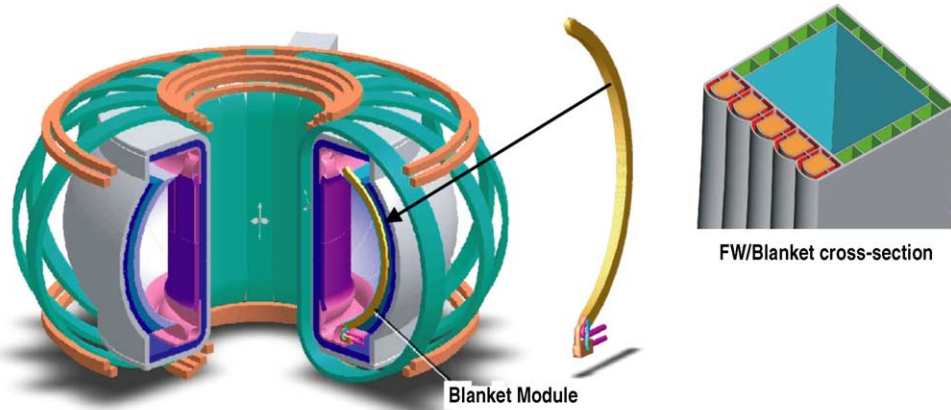
Fig. 7. APEX re-circulating blanket tokamak reactor, poloidal module and FW/blanket cross-section.

the T_{max} of AFS and the inboard design is limited by interface temperature between FLiBe and AFS, and the over all thermal performance is further constrained by the interface temperature limit between Pb and AFS. Without including the MHD effect, the inboard and outboard total pressure drops are 0.41 and 0.84 MPa, respectively. More detailed thermal-hydraulics analy-
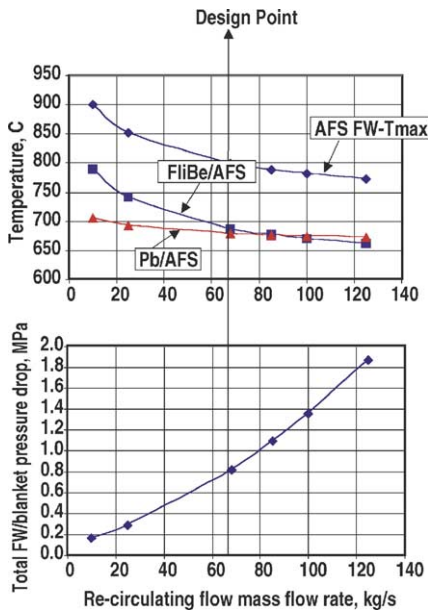
Fig. 8. FW maximum and material interface temperatures (FLiBe/AFS, Pb/AFS), and total FW/blanket pressure drop vs. re-circulating flow (stream B) mass flow rate.
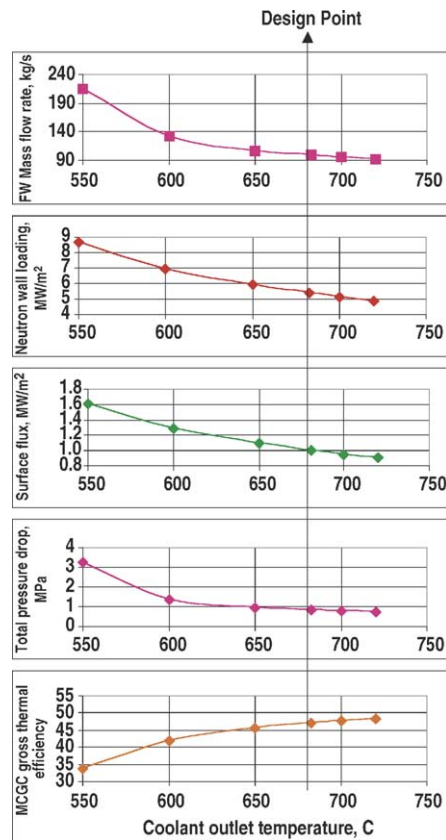
Fig. 9. Design variations with coolant T_{out} with selected FW/blanket configuration and T_{max}-AFS < 800 °C, and coolant tin = 500 °C.

sis of the blanket design and with the inclusion of MHD effect is given in Section 6.

5.4. Systems analysis

For an integrated performance assessment of the FW/blanket design, we made use of a systems code [18] to provide consistency of the design with a tokamak power reactor. The code calculation starts with the specification of plasma aspect ratio, elongation and bootstrap fraction, the physics parameters of normalized beta, total beta and polodial beta can then be calculated. With the selection of the central column toroidal field coil conductor radius (R_c) and inboard coil stand-off distance (d_{IB}), the major radius (R_o) and the geometry of the reactor plasma toroidal chamber can be specified. With the assumption of the plasma triangularity at 0.4 and a scrape-off distance of 5 cm at the inboard and outboard midplane, the geometry of the plasma can also be specified. With the additional selection of the central column current density (J_c) for a superconducting coil machine, the toroidal magnetic field strength, plasma ion density and reactor reactivity can be calculated. The option of adding impurities into the core to enhance the radiation of transport power was exercised in order to reduce the heat flux at the divertor and then determine the heat flux at the first wall. Energy balance was then performed to account for the first wall and divertor heat flux, average neutron wall loading, and re-circulating power of the reactor design. For this exercise the variation of aspect ratio was used to study the variation on first wall heat flux. A maximum outboard midplane maximum surface heat flux of 1 MW/m^2 was selected as the design point. This analysis allows us to provide a consistent set of design and geometric parameters for reactor and FW/blanket designs with the selected structural and blanket coolant materials. Results are tabulated in Table 6.

Results show that with the assumption of selected impurities in the core, a radiation fraction of 56% can be obtained. This allows the design of a tokamak reactor with a maximum outboard surface heat flux of 1 MW/m^2. The corresponding average neutron wall loading is 3.8 MW/m^2, with a fusion power output of 2755 MW. Using MCGC as the power conversion cycle [19], with the coolant inlet/outlet coolant temperature of 500/681 °C, a gross thermal efficiency of 47% can be

projected as shown in Section 7. This leads to a reactor net power output of 1289 MW-electric.

5.5. Conclusions

We performed a parametric thermal-hydraulics and systems calculation assessment on the AFS structural material and FLiBe coolant blanket and found that the maximum surface loading that the first wall can be designed to is about 1 MW/m^2. The corresponding average neutron wall loading is 3.8 MW/m^2. We found by adjusting the re-circulation flow mass flow rate, that the inboard blanket temperatures can be adjusted to be similar to the outboard blanket, even though the outboard blanket is limited by the T_{max} of AFS and the inboard design is limited by the interface temperature between FLiBe and AFS, and the over all thermal performance is further constrained by the interface temperature limit between Pb and AFS. Experimental confirmation will be needed to demonstrate compatibility between Pb and AFS at temperature ∼700 °C. Including the first wall heat flux, with a coolant exit temperature from the power conversion system at 500 °C, the coolant outlet temperature from the central FLiBe column becomes 681 °C. When coupled to an MCGC as shown in Section 7 a gross thermal efficiency of 47% can be projected leading to a net electricity output of 1289 MWe.

6. Thermal-hydraulics

Section 5 shows the feasibility and potential performance of the AFS/FLiBe FW/blanket design without the inclusion of MHD effects. In the following MHD effects are taken into account and more detailed thermal-hydraulics analysis of the first wall design are also presented.

6.1. MHD effects on FLiBe flow in the re-circulating blanket

The goal of this section is to qualify and quantify the MHD effects related to the FLiBe flow in the re-circulating blanket under a strong magnetic field and to give directions for calculating the MHD pressure drop in the subsequent thermal-hydraulics analysis. Considerations have been given to the front and side channels
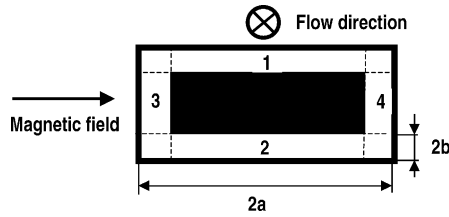
Fig. 10. Schematic for the front channel flow: (1) front sub-channel; (2) back sub-channel; (3) and (4) side sub-channels.

as well as the central channel for both the inboard and outboard regions and cover the following three issues:

- turbulence suppression by a magnetic field;
- effect of the magnetic field on heat transfer;
- MHD pressure drop.

The basic dimensionless parameters related to the MHD analysis is the Hartmann number ($Ha = B_0 a(\sigma/\nu\rho)^{0.5}$), and the Reynolds number ($Re_D = U_0 D/\nu$), where D is the hydraulic diameter, U_0 the flow velocity, σ the electrical conductivity, ρ the density and ν the kinematic viscosity. In all cases the channels are treated as straight ducts of a rectangular cross-section, $2a \times 2b$ with $L = 8$ m as the flow length. Here "a" is the half of the channel dimension in the direction of the applied (toroidal) magnetic field. The flow is considered as fully developed over the whole length. The entry/exit effects as well as the field non-uniformity effects at the flow extremities have not been taken into account. One more parameter is the wall conductance ratio, which is $c_w = t_w \sigma_w / a\sigma$, where t_w is the wall thickness. Since electrical conductivity of the structural wall σ_w is about 10^4 higher than that of FLiBe, the condition $c_w \gg 1/Ha$ is always satisfied, thus the ducts can be considered as perfectly conducting. In the analysis, the first wall channel can be subdivided into four sub-channels (Fig. 10), which we will refer to as the front and back sub-channels (1 and 2) and two side sub-channels (3 and 4). The dimensional and dimensionless parameters for different flows are shown in Table 7.

6.1.1. Effect of the magnetic field on turbulence

In a magnetic field, turbulence is dampened due to the Joule dissipation. This is accompanied by heat transfer degradation. The degree of turbulence suppression generated by a magnetic field depends on the field orientation. Based on the experimental data for MHD flow in rectangular channels in a spatially distributed magnetic field, the flow becomes fully laminar if the parameter Ha/Re is higher than about 0.008 [20]. Strictly speaking, this value was evaluated for channels with electrically non-conducting walls. Flow laminarization in channels with conducting walls has not been studied in detail. However, in [20], the author suggests the same criterion can be applied to the flows in electrically conducting channels. This approach is not fully consistent with general observations of intense vorticity suppression in electrically conducting channels due to higher Joule dissipation. Anyway, in the present analysis, we followed the general practice applying the standard criterion, even though the channel walls are good conductors. The conclusions on the turbulence suppression should be revised, once new data on turbulence suppression become available.

For the flow in the central channel at the inboard, the criterion (Ha/Re) > 0.008 is satisfied (see Table 7). Therefore, this flow will be laminar. One can also expect high turbulence suppression in the central channel flow at the outboard, where $Ha/Re = 0.006$. As for the other channels, $Ha/Re \ll 0.008$. This indicates negligible or small effect of the magnetic field on the fluid flow and even less impact on the turbulence. Detailed calculations using the "K-epsilon" model of turbulence for MHD flows [21] have confirmed that in the FLiBe flows in the front and side channels, turbulence suppression does not exceed several percent. However, the model used does not implement any effects due to conducting walls either. Hence, the uncertainty with the wall electrical conductivity still remains.

6.1.2. Effect of a magnetic field on heat transfer

Data on heat transfer measurements is also seen in the literature for both liquid metals and, to a lesser extent, strong electrolytes in a magnetic field. For FLiBe, the most appropriate data will be those associated with the electrolyte since both have a high Prandtl number and the heat transfer is dominated by turbulent convection. The following correlation is given by Blums [22]:

$$\frac{Nu}{Nu_0} = 1 - 1.2N_D, \tag{1}$$

Table 7
Basic parameters in the reference FLiBe flows

Flow parameter	Inboard	Outboard
Front channel		
Magnetic field (T)	7.8	4.3
a (m)	0.0035 (3 and 4)	0.0035 (3 and 4)
	0.025 (1 and 2)	0.025 (1 and 2)
b (m)	0.025 (3 and 4)	0.025 (3 and 4)
	0.0035 (1 and 2)	
$\beta = b/a$	7.14 (3 and 4)	7.14 (3 and 4)
	0.14 (1 and 2)	0.14 (1 and 2)
FLiBe velocity (m/s)	3.6	6.4
Ha	2.77 (3 and 4)	1.53 (3 and 4)
	19.8 (1 and 2)	10.9 (1 and 2)
Re	1658 (3 and 4)	2947 (3 and 4)
	11842 (1 and 2)	21052 (1 and 2)
Ha/Re	0.001670	0.00052
Side channel		
Magnetic field (T)	7.8	4.3
D (m)	0.0261	0.0261
FLiBe velocity (m/s)	1.49	2.75
Ha_D	20.7	11.4
Re_D	7392	13505
Ha_D/Re_D	0.0028	0.00084
Central channel		
Magnetic field (T)	7.8	4.3
D (m)	0.218	0.218
FLiBe velocity (m/s)	0.2	0.33
Ha_D	172.6	95.1
Re_D	9745	15869
Ha_D/Re_D	0.0177	0.006

where $N_D = Ha_D^2/Re_D = \sigma D B_0^2/\rho U_0$ is the interaction parameter (based on the hydraulic diameter of the duct). Nu and Nu_0 are the two Nusselt numbers with and without a magnetic field, respectively. This correlation predicts the approximate percentage decrease in the heat transfer due to suppression of turbulent eddies by the magnetic field. It has been validated for the MHD turbulent flows with $N_D < 1$. This is the regime of interest for reference flows using FLiBe. One can see that for both front and side channels the reduction in Nu is insignificant. The same conclusions on heat transfer degradation agree well with the K-epsilon calculations. However, using Blums' formula and the present version of the K-epsilon model for perfectly conducting channels may result in underestimation of heat transfer degradation because of the same reasons mentioned in the previous section.

6.1.3. MHD pressure drop

In the reference flow (except for the central channel flows, where the flow is laminar), the pressure drop is the sum of the MHD pressure drop and the pressure drop due to wall friction in turbulent flow. In terms of the pressure gradient, $-\mathrm{d}P/\mathrm{d}x$, it can be written as

$$\left(-\frac{\mathrm{d}P}{\mathrm{d}x}\right)_{\text{total}} = \left(-\frac{\mathrm{d}P}{\mathrm{d}x}\right)_{\text{MHD}} + \left(-\frac{\mathrm{d}P}{\mathrm{d}x}\right)_{\text{turb}}. \quad (2)$$

As a reasonable approximation, the two terms on the RHS of the expression can be calculated independently. As for the second term on the RHS of the expression, it is calculated using general formulas for non-MHD frictional turbulent flows assuming that the turbulence suppression by a magnetic field is small. The first term,

in turn, can be decomposed into three different components:

$$\left(-\frac{\mathrm{d}P}{\mathrm{d}x}\right)_{\mathrm{MHD}} = \left(-\frac{\mathrm{d}P}{\mathrm{d}x}\right)_{\mathrm{L}} + \left(-\frac{\mathrm{d}P}{\mathrm{d}x}\right)_{Ha} + \left(-\frac{\mathrm{d}P}{\mathrm{d}x}\right)_{\mathrm{S}}, \qquad (3)$$

where the first component stands for the MHD drag on the flow due to the Lorentz force, while the other two are responsible for the viscous friction in the Hartmann layers and in the side layers, respectively. Using (3), the formula for the pressure gradient can be rewritten in the following way:

$$\left(-\frac{\mathrm{d}P}{\mathrm{d}x}\right)_{\mathrm{total}} = \underbrace{\left(-\frac{\mathrm{d}P}{\mathrm{d}x}\right)_{\mathrm{L}}}_{\text{Lorentz force}}$$

$$+ \underbrace{\left\{\left(-\frac{\mathrm{d}P}{\mathrm{d}x}\right)_{Ha} + \left(-\frac{\mathrm{d}P}{\mathrm{d}x}\right)_{\mathrm{S}} + \left(-\frac{\mathrm{d}P}{\mathrm{d}x}\right)_{\mathrm{turb}}\right\}}_{\text{viscous friction}}, \quad (4)$$

where the second term on the RHS represents the drag effect due to viscous friction. It should be noted that separating the viscous drag into three different components in formula (4) and calculating them independently might overestimate the pressure gradient especially if the level of turbulence is not high. Rather than that, a more rigorous technique would be to calculate the term $(-\mathrm{d}P/\mathrm{d}x)_{\mathrm{viscous\,friction}}$ as a whole using a full set of the equations for MHD turbulence. Unfortunately, such an approach is not available at present.

One of the approximate approaches for estimating the MHD pressure drop is using an analytical formula for perfectly conducting channels by Chang and Lundgren [23], which is as follows:

$$\left(-\frac{\mathrm{d}P}{\mathrm{d}x}\right)_{\mathrm{MHD}}$$

$$= \sigma U_0 B_0^2 \frac{1}{1 - (1/Ha) - (2.4/Ha^{3/2}\beta)}. \qquad (5)$$

Three different terms in the denominator of (5) stand for the drag in the flow core due to the Lorentz force, Hartmann friction, and the side layer friction respectively. The formula gives accurate predictions of the MHD drag if $Ha \gg 1$. In the limit of very

Table 8
Coefficient K in formula (6) for front/back and side sub-channels of the front channel

	Inboard	Outboard
Front/backsub-channel		
K [20]	12490	6634
K (code)	13682	6979
Side sub-channels		
K [20]	16631	17352
K (code)	15213	7525

high Hartmann number, $(-\mathrm{d}P/\mathrm{d}x)_{\mathrm{MHD}} = \sigma U_0 B_0^2$ would work very well for liquid metals in a strong magnetic field.

For the FLiBe flow in the front channels, the assumption $Ha \gg 1$ is more or less valid only for inboard front/back and side sub-channels flows. For the flow at the outboard side sub-channels, $Ha = \mathrm{O}(1)$ so that formula (5) is not applicable there, and it is more appropriate to do numerical calculations.

As a numerical tool, we used a 2D computer code for the fully developed MHD flows in rectangular ducts [24]. The code is applicable to MHD flows without any restrictions on the Hartmann number. The comparisons using the code have shown good agreement with the results based on formula (5) for the front channel inboard flows (discrepancy was within 10%). For the outboard flow in the side sub-channels, the discrepancy was tens of percents.

The results of calculations performed with the code and formula (5) for the front and side sub-channels of the front channel for the parameters listed in Table 7 are presented in the following form:

$$\left(-\frac{\mathrm{d}P}{\mathrm{d}x}\right)_{\mathrm{MHD}} = KU_0. \qquad (6)$$

In (6) the velocity has a unit of m/s, and the pressure gradient is of N/m^3. The data for the coefficient K are summarized in Table 8. They can be used in thermal-hydraulics analysis to estimate the MHD pressure drop.

6.1.4. Conclusions

1. Turbulence suppression by a magnetic field and heat transfer degradation in the flows through the side and front channels is insignificant for both inboard and outboard first wall.

2. The flow through the central channels is fully laminar at the inboard and almost laminar at the outboard.
3. Analysis of the effect of electrically conducting walls on turbulence suppression by a magnetic field should be performed for more reliable estimations of the impact of MHD turbulence on the design.
4. Formulas for MHD pressure drop for sub-channels of the front channel have been obtained on the basis of the 2D theory for both the inboard and outboard.
5. More detailed estimations of the MHD pressure drop will require addressing 3D MHD effects related to changes of the flow geometry and magnetic field variations.

6.2. First wall thermal-hydraulics optimization

Scoping heat transfer calculations without the inclusion of MHD effects and results are presented in Section 5. This was used to define the FW/blanket design flow configuration. With the inputs from Section 6.1, MHD effects can be included and the parametric thermal analysis of the first wall is presented in the following section.

6.2.1. Design configuration
Parametric thermal-hydraulics analysis was performed to optimize the first wall (FW) tubes design of the re-circulating flow blanket. The reference FW design utilizes rectangular channels as shown in Fig. 11. Another FW design option considered employs circular tubes with a conformed strong back, as shown in Figs. 12 and 13.

6.2.2. Calculational procedure
We assessed the optimum design by varying the eccentricity location of the Pb tubes in the FW channels for both the circular and rectangular design options. The FW channel dimensions were optimized to maintain uniform pressure drop (including MHD pressure drop) and uniform FLiBe temperature around the Pb multiplier tube. We determined the FW thermal-hydraulics parameters (pressure drop, velocities, temperatures) for the reference rectangular FW channels. Table 9 lists the formulas used in the heat transfer and pressure drop calculations [25,26]. The MHD pressure drop was calculated using formulas and methods explained in Section 6.1. Table 10 gives the FLiBe prop-
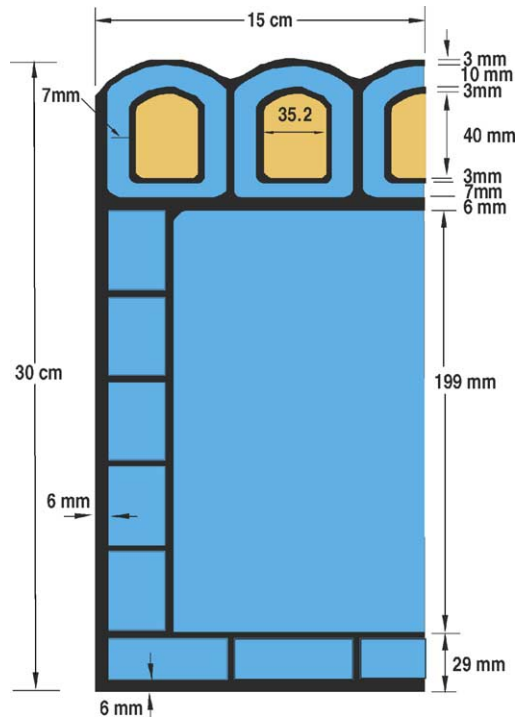
Fig. 11. FW configuration of the re-circulating blanket with rectangular channels.
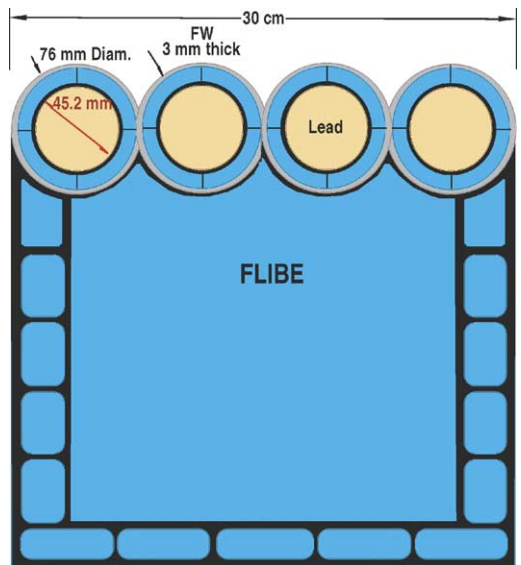
Fig. 12. Re-circulating blanket with circular FW tubes.
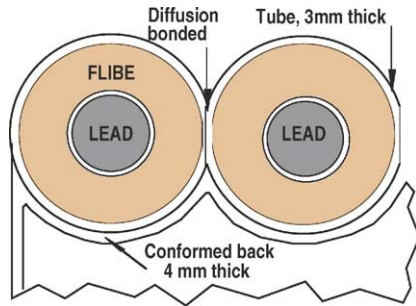
Fig. 13. FW tubular configuration.

Table 9
Formulas used in thermal-hydraulics analysis[a]

The Nusselt number	$Nu = 0.0118Pr^{0.3}Re^{0.9}$, for $Pr > 20$
The Blasius friction coefficient	$f = 0.3164/Re0.25$
Pressure drop in a vertically moving fluid	$\Delta P = \rho v^2/2 + f\rho Lv^2/2d$

[a] Nu is the Nusselt number; Pr the Prandtl number; Re the Reynolds number; ρ the fluid density; v the coolant velocity; d the coolant tube hydraulic diameter; L the coolant tube length.

erties used in the calculations. The radial variation of nuclear heating in the different constituents of the blanket is given in Fig. 3. The results are normalized to a unit neutron wall loading. These profiles were modified by the appropriate neutron wall loading values in the IB and OB regions.

6.2.3. Impact of using eccentrically located lead tubes

Using eccentrically located lead tubes in the FW results in larger cooling sub-channels at the front and smaller ones at the back. For the same pressure drop, the flow velocity will be larger with higher heat transfer coefficient at the front where a larger heat load needs to be removed. We assessed this effect for circular FW tubes. The velocity profile around the Pb tube with eccentricity of 4.33 mm is shown in Fig. 14. This leads to the same frictional pressure drop (0.585 MPa) and

Table 10
FLiBe properties at 600 °C

Density, $\rho = 2120 \, \text{kg/m}^3$
Thermal conductivity, $k_{th} = 1 \, \text{W/mK}$
Heat capacity, $C_p = 2380 \, \text{J/kg K}$
Kinematics viscosity, $\nu = 5.48\text{e}^{-6} \, \text{m}^2/\text{s}$
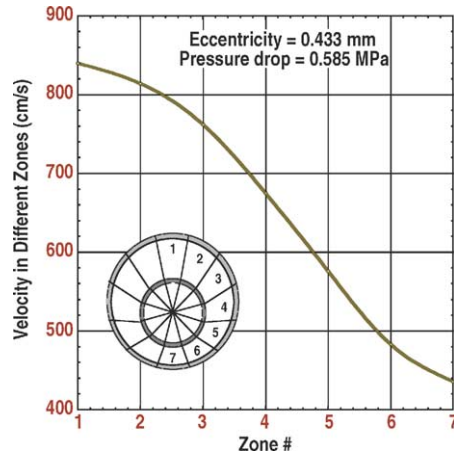
Fig. 14. Local FLiBe velocity distribution around an eccentric Pb tube.

FLiBe temperature rise (30 °C) at the front and back. Notice that if concentric tubes are used, the FLiBe velocity will be uniform around the Pb tube with a value of only 7.2 m/s. In addition, the eccentric configuration enhances the FLiBe temperature uniformity around the Pb tube as indicated by comparing the results in Figs. 15 and 16. This has the advantage of reducing the expected thermal stresses. Figs. 17 and 18 also show that using eccentric tubes reduces the maximum interface temperature between the FLiBe and steel.
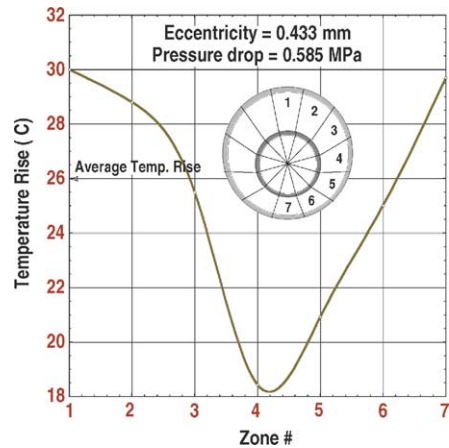
Fig. 15. Local FLiBe temperature rise distribution around the eccentric Pb tube.
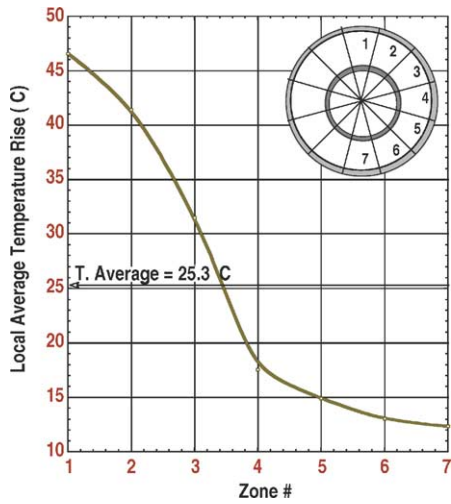
Fig. 16. Local FLiBe temperature rise distribution around the concentric Pb tube.

6.2.4. Analysis of the reference rectangular outboard FW tubes

The design with circular FW tubes is easier to fabricate. Stress calculations for a blanket element, taking into account the coolant pressure in the FW channels as well as the pressure in the large central duct showed that the stresses caused by the pressure in the FW tube itself are lower for the circular tubes. However, the pressure in the central duct leads to higher stresses in the FW region compared to the rectangular reference design. For
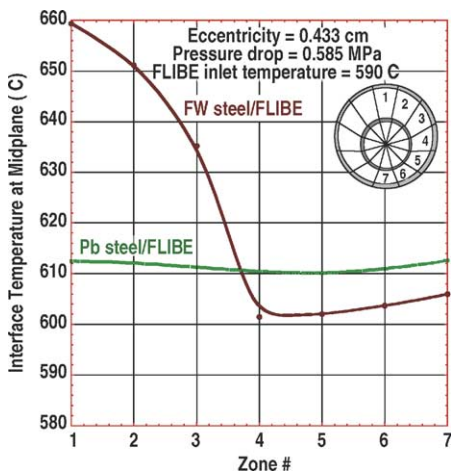
Fig. 17. Interface temperatures between FLiBe and steel around the eccentric tube.
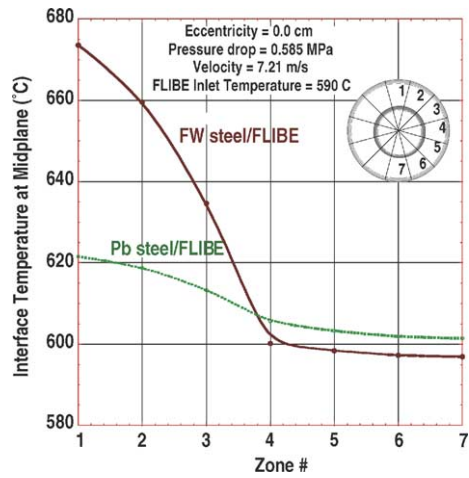
Fig. 18. Interface temperatures between FLiBe and steel around the concentric tube.

this reason the rectangular FW channel configuration is considered as the reference design.

Similar to the circular FW tube option, we optimized the reference rectangular FW tube design by varying the eccentricity (e) of the multiplier tube and adjusting the width (W) of the side FLiBe zone, as shown in Fig. 19. The magnetic field at the outboard blanket is ~4.3 T. The MHD pressure drop was included using the results reported in Section 6.1. Fig. 19 shows the FW model of the reference rectangular design used in the calculations. Fig. 20 shows the optimization results of the reference rectangular design with the optimum eccentricity of 0.357 cm. Also the width of the
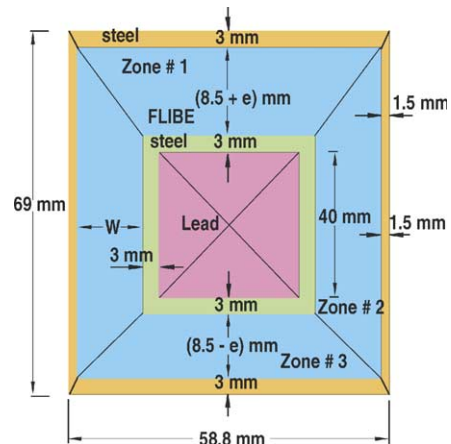
Fig. 19. The FW model used in the calculations.
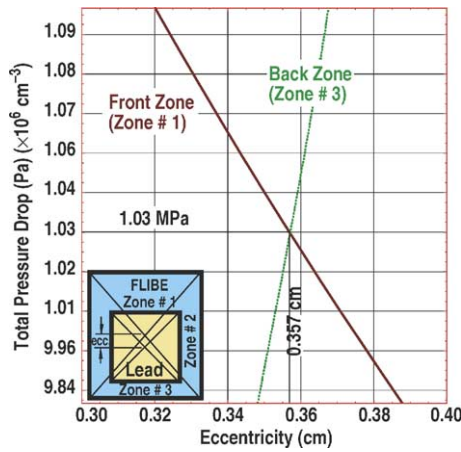
Fig. 20. The outboard FW total pressure drop (MHD and frictional) and optimum eccentricity.

side zone (W) was varied to maintain a uniform FLiBe temperature rise leading to higher FW coolant outlet temperature.

The widths of the FLiBe zones surrounding the Pb tube optimized to maintain uniform pressure drop and temperature rise are given in Table 11. The total pressure drop (MHD and frictional) is 1.03 MPa. The volumetric flow rate per tube is 9043 cm^3/s. The FLiBe flow area at midplane per tube is 14.1 cm^2 resulting in an average FLiBe velocity at midplane of 6.42 m/s and total FLiBe temperature rise of 30 °C. Table 12 gives the maximum interface temperatures for the optimized OB FW. The maximum interface temperature between the FLiBe and FW steel is 667 °C and the maximum interface temperature between lead and steel is 680 °C.

6.2.5. Analysis of the reference rectangular inboard FW tubes

We optimized the reference inboard rectangular FW design in a way similar to that previously described for the outboard FW. The magnetic field is ~7.8 T which is much higher than that in the outboard FW. However, the heat loads are lower than those in the OB region.

Fig. 21. The inboard FW total pressure drop (MHD and frictional) and optimum eccentricity.

Fig. 21 shows the optimization results of the reference IB rectangular design with the optimum eccentricity of 0.483 cm.

The widths of the FLiBe zones surrounding the Pb tube optimized to maintain uniform pressure drop and temperature rise are given in Table 13. The total pressure drop (MHD and frictional) is 0.88 MPa. The volumetric flow rate per tube is 6287 cm^3/s. The FLiBe flow area at midplane per tube is 13.4 cm^2 resulting in an average FLiBe velocity at midplane of 4.69 m/s and total FLiBe temperature rise of 30 °C. Table 14 gives the maximum interface temperatures for the optimized OB FW. The maximum interface temperature between the FLiBe and FW steel is 686 °C and the maximum interface temperature between lead and steel is 652 °C.

The heat loads handled by the IB FW are smaller than those for the OB FW. In addition, the poloidal profile of the surface heat flux is more uniform than that for the volumetric nuclear heating. Also the MHD effects are higher at the IB FW than the OB FW because of the much larger magnetic field. These differences result in

Table 11
Pressure drop for optimized OB FW

Zone number	Width (mm)	FLIBE velocity (m/s)	MHD pressure drop (MPa)	Frictional pressure drop (MPa)
1	12.07	8.9	0.32	0.71
2	5	4.6	0.41	0.62
3	4.93	4.46	0.44	0.59

Table 12
Maximum interface temperatures for optimized OB FW

Zone number	Re	h (W/m^2 K)	Interface temperature between FLiBe and outer steel (°C)	Interface temperature between FLiBe and inner steel (°C)	Interface temperature between lead and steel (°C)
1	39195	18003	667	630	680
2	8394	10858	611	637	660
3	8017	10566	611	633	662

Table 13
Pressure drop for optimized IB FW

Zone number	Width (mm)	FLIBE velocity (m/s)	MHD pressure drop (MPa)	Frictional pressure drop (MPa)
1	13.33	6.11	0.552	0.328
2	4.25	3.13	0.509	0.371
3	3.67	3.38	0.354	0.526

a larger eccentricity being required in the IB FW. Furthermore, lower velocities and frictional pressure drop are obtained in the IB FW. While the higher magnetic field results in higher MHD pressure drop in the IB FW, the total pressure drop is lower than that in the OB FW. Because the total pressure drop in the IB and OB are different, we should have a separate cooling loop for each of them.

7. Power conversion system

Candidate power conversion systems in fusion power plants are based either on the Rankine cycle (employing steam turbines) or on the Brayton cycle (employing closed cycle helium gas turbines). The usual domain for steam turbines is coolant temperature up to 600 °C; closed cycle helium turbines are considered for temperatures above 700 °C. For the application in fusion power plants the temperature range for the Brayton cycle has been reduced to ~650 °C by selecting a maximum helium pressure >12 MPa [27] and to ~600 °C by using multiple turbine stages [19].

Closed cycle helium turbines are under development for application in high temperature fission power plants. Recent commercialization of magnetic bearings for large turbo-machinery increased their feasibility and attractiveness, promising lower capital costs than comparable steam turbine systems, due to their higher power density. As shown by Peterson [19], an efficiency of >45% can be achieved with the Brayton cycle at maximum helium temperatures of 650 °C. This is comparable to modern steam turbine plants. However, there are additional reasons why the Brayton cycle has been selected for a fusion power plant based on FLiBe-cooled blankets.

7.1. Mitigation of tritium control

The solubility of tritium in FLiBe is exceptionally low, resulting in high tritium partial pressure in this fluid. This implies, together with the high FLiBe temperatures, large tritium permeation rates in the heat exchanger between the primary FLiBe loop and the secondary coolant loop to the power conversion system.

Table 14
Maximum interface temperatures for optimized IB FW

Zone number	Re	h (W/m^2 K)	Interface temperature between FLiBe and outer steel (°C)	Interface temperature between FLiBe and inner steel (°C)	Interface temperature between lead and steel (°C)
1	29703	12701	686	629	652
2	4860	7812	611	634	644
3	4530	8491	610	627	638

In a system with steam turbines without an intermediate heat transport loop between blanket and power conversion system, tritium permeation into the steam would be intolerably high since tritium extraction from the huge mass of water/steam is not practicable (isotopic separation required). An intermediate heat transport loop would increase capital costs and could lower the achievable thermal efficiency.

In case of a Brayton cycle, tritium permeates in a recuperator from the coolant into the secondary helium where it would be easier to extract. In this secondary loop the only walls in contact to the environment are the low temperature heat exchanger of the heat sink and the intercooler of the compression stages. The wall temperatures there are below 100 °C, reducing in this way tritium permeation losses to the cooling water by orders of magnitudes. A further reduction to easily tolerable values is possible if aluminum alloy tubes are used in these heat exchangers.

It should be noted that the design and power generation from the divertor of the tokamak reactor have not been included in our consideration.

7.2. Eliminating the potential for coolant/water reaction

If a tube rupture in the steam generators of a Rankine cycle is postulated, the high steam pressure could lead to tube ruptures in the blanket. This would be especially a significant safety issue for liquid metal breeder blankets, or if beryllium is used as the neutron multiplier. Since FLiBe is less reactive with water, and the beryllium is used here only outside the blanket for chemistry control, the risk for damaging water/coolant (or water/beryllium) reactions is considerably lower, but nevertheless these will have to be investigated in detail.

7.3. Molten salt coolant gas cycle system

The molten salt coolant gas cycle (MCGC) uses multiple, modular turbo-compressor-generator units in a closed cycle allowing multiple stages of reheating and intercooling [19]. The MCGC could also greatly simplify the control of tritium, a particular benefit when FLiBe is used as the coolant as mentioned above. The molten salt coolant from the FW/blanket is the heat source for the helium system driving the modular turbines. The Brayton cycle includes a recuperator, multiple intercoolers and compressors, and multiple turbines and heaters.

We evaluated different applications of the MCGC. The following input parameters are selected for the purpose of this comparison:

Ratio of specific heats (γ)	1.66
Recuperator effectiveness (%)	95
Turbine efficiency (%)	93
Compressor efficiency (%)	89
System pressure loss ($\Delta P/P_{n+1}$)	0.07

Before entering a compressor, the helium gas is cooled in what is called either a precooler or an intercooler. The gas temperature exiting these coolers is the lowest temperature in the MCGC and is fixed in this comparison to 35 °C. The molten salt coolant from the fusion energy system is used to heat the helium gas to temperature T_a, which is set at 660 °C. This helium gas then passes through one or more turbines where the gas expands and reduces to a temperature T_b, which is set at 480 °C.

A fairly straightforward arrangement used in the GT-MHR has one turbine and two compressors on a single shaft with the precooler and intercooler all contained within a pressure vessel. The GT-MHR arrangement also places the recuperator within the same pressure vessel. For the fusion energy temperatures evaluated in Table 15, the thermal efficiency of a two compressor ($n = 2$) and one turbine ($m = 1$) arrangement is 41.7%, which is 7.2% higher than if there was only one compressor ($n = 1$, $m = 1$). The maximum pressure ratio in this system is 1.93. High system pressures have positive and negative consequences. Higher pressures increase the gas density thereby reducing the velocity or flow area required to provide a given mass flow rate. Higher pressures also increase the material requirements of pressure vessels and other internal structures that have high pressure differentials.

The system pressure ratio increases to 3.46 when the number of turbines and molten salt coolant heat exchangers is two. Comparing the case with two compressors one notes that adding a turbine set also increases the thermal efficiency by 5.5–44%. Such a system arrangement might also include two generators with each turbine coupled to its own compressor and generator.

Table 15
Evaluation of turbine and compressor combinations for the MCGC

	n, m	T_a (°C)	T_b (°C)	P_{n+1}/P_1	η (%)
Four compressors, three turbines	4, 3	660	480	6.2	47.3
Three compressors, three turbines	3, 3	660	480	6.2	45.8
Four compressors, two turbines	4, 2	660	480	3.46	46.9
Three compressors, two turbines	3, 2	660	480	3.46	45.9
Two compressors, two turbines	2, 2	660	480	3.46	44.0
Three compressors, one turbine	3, 1	660	480	1.93	42.6
Two compressors, one turbine	2, 1	660	480	1.93	41.7
One compressor, one turbine	1, 1	660	480	1.93	38.9

An arrangement of three compressors and two turbines is not practical but one with four compressors and two turbines would be possible by simply adding an additional compressor and intercooler to each turbine-generator set of the two compressors–two turbines arrangement. This hardware addition results in no change in the system pressure ratio but does increase thermal efficiency by 6.6–46.9%. There is no further benefit from adding more turbine generator sets.

Table 16 shows three potential system arrangements. The benefit of increased thermal efficiency has to be weighed against the increase in capital cost associated with a system with more major pieces of equipment. The additional equipment would be of a smaller size since the heat or work duty of that equipment

$$P_m \leq \begin{cases} S_m \text{ at thickness-averaged temperature,} \\ S_t \text{ at thickness-averaged temperature and design life,} \end{cases} \tag{7}$$

is now being shared.

For our design we have selected the two turbines and four compressors design with each turbine handling 800 MW$_{th}$. For the reactor we will need two of this power conversion system to handle the total thermal power of 3200 MW$_{th}$, and with a gross thermal efficiency of 46.9%.

8. Heat conduction and stress analyses

Heat conduction and elastic stress analyses were carried out for the reference blanket design, using the finite element program ABAQUS [28]. The cross-section of the blanket is shown in Fig. 22. The thermal-hydraulic parameters are reproduced in Table 17. Unit-poloidal-thickness slices at the bottom, midplane, and the top of the blanket were analyzed. No heat conduction was

assumed to occur in the poloidal direction. The stress analyses were conducted with the generalized plane strain assumption.

A summary of the temperatures and stresses in the blanket is given in Table 18. Because of the high pressure, the primary stresses are highest at the bottom of the blanket. On the other hand, because of the high surface heat flux, the temperatures and thermal stresses are highest at the midplane. Details of this analysis are presented in reference [6]. The last two columns in Table 18 contain the time-independent primary stress allowable S_m and the time-dependent primary stress allowable S_t. The primary stress limits for the membrane (P_m and P_L) and bending (P_b) components are as follows:

$$P_L + P_b \leq K S_m, \tag{8}$$

and

$$P_L + \frac{P_b}{K_t} \leq S_t, \tag{9}$$

where K is the bending shape factor ($=1.5$) and $K_t = (K + 1)/2$. A design life of 2 years was used for this study. An examination of Table 18 shows that the first wall satisfies all of the primary stress limits. A plot of the peak primary membrane plus bending stress at the bottom of the blanket is shown in Fig. 23. It is evident that the maximum primary stress (182 MPa) occurs not at the first wall but at the back wall of the first wall channel. However, since the average temperature of the back wall of the first wall channel is relatively low (630 °C), the allowable stresses are correspondingly higher and the primary stress limits are satisfied [29].

Table 16
Potential system arrangements

Number of major pieces of equipment			P_{n+1}/P_1	η (%)
One turbine-generator	Two compressors	One recuperator	1.93	41.7
One molten salt coolant HX	Two water HXs			
Two turbine-generators	Two compressors	One recuperator	3.46	44
Two molten salt coolant HXs	Two water HXs			
Two turbine generators	Four compressors	One recuperator	3.46	46.9
Two molten salt coolant HXs	Four water HXs			

Table 17
Thermal-hydraulic parameters

	First wall channel	Back and side channels	Central channel
Bottom			
Neutron $\Gamma_n = 2.8\,\text{MW/m}^2$			
Heat flux, $\phi = 0.8\,\text{MW/m}^2$	14	7	7
Power density (W/cm³)			
T_{bulk} (°C)	586	625	683
Absolute pressure (MPa)	1.4	0.26	0.36
Heat transfer coefficient (W/m² °C)	16998 (front), 13395 (side), 10285 (back)	8431	1087
Midplane			
Neutron $\Gamma_n = 5.38\,\text{MW/m}^2$			
Heat flux, $\phi = 1.0\,\text{MW/m}^2$	26.9	13.5	13.5
Power density (W/cm³)			
T_{bulk} (°C)	601	620	649
Absolute pressure (MPa)	0.8	0.23	0.28
Heat transfer coefficient (W/m² °C)	17957 (front), 13395 (side), 10285 (back)	8434	1088
Top			
Neutron $\Gamma_n = 2.8\,\text{MW/m}^2$			
Heat flux, $\phi = 0.8\,\text{MW/m}^2$	14	7	7
Power density (W/cm³)			
T_{bulk} (°C)	616	616	616
Absolute pressure (MPa)	0.2	0.2	0.2
Heat transfer coefficient (W/m² °C)	18934 (front), 13395 (side), 10285 (back)	8445	1090

Table 18
Summary of first wall temperatures and stresses

First wall location	Wall temperature (°C)		Primary stress intensity (MPa)		Secondary stress intensity, Q (MPa)	S_m (MPa)	S_t[a] (MPa)
	Average	Peak	Membrane (P_m)	Membrane + bending ($P_L + P_b$)			
Bottom	673	711	14	130	195	160	260
Midplane	709	758	10	90	283	125	240
Top	698	737	3	30	248	130	245

[a] Corresponds to 2-year lifetime at average wall temperature.

Table 19
First wall primary plus secondary stress limits

First wall location	Average wall temperature[a] (°C)	Yield stress (MPa)	$X = (P_L + P_b/K_t)/S_y$	$Y = \Delta Q/S_y$
Bottom	630	400	0.27	0.49
Midplane	650	350	0.20	0.80
Top	640	360	0.07	0.69

[a] Average temperature during plasma-on and plasma-off conditions.
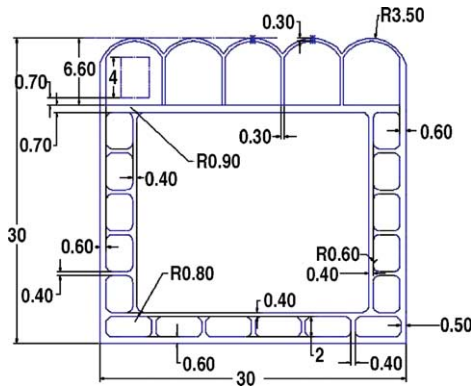
Fig. 22. Re-circulating blanket cross-section (dimension in cm).

The maximum thermal stress (Q) occurs at the mid-plane of the blanket and its distribution was calculated [6]. A simple but conservative rule for meeting the primary plus secondary stress limit for cyclic ratcheting is the Test A2 of the ITER structural design criteria (ISDC), which is as follows:

$$X + Y \leq 1, \tag{10}$$

where

$$X = \frac{P_L + P_b/K_t}{S_y}, \tag{11}$$

$$Y = \frac{\Delta Q}{S_y}, \tag{12}$$
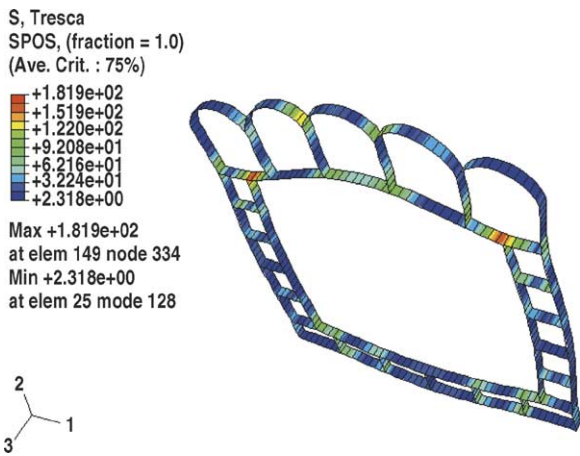
Fig. 23. Primary membrane plus bending stress distribution at the bottom of the blanket.

and S_y is the average temperature of the section during the secondary stress cycle, i.e., during plasma-on and plasma-off conditions, and ΔQ is the secondary stress intensity range during the cycle. Table 19 shows that the stresses in the blanket at the bottom, midplane and top satisfy Eq. (10).

The time-dependent (2-year design life) and time-independent primary stress limits for 12YWT (AFS steel) are satisfied by the reference blanket design. The primary plus secondary stress limit is also satisfied at the bottom, midplane, and top of the blanket. These results are based on the maximum temperature of the first wall at 758 °C. With this temperature, the stress analyses results are based on the most conservative ratcheting rule in the code. As shown the more detailed thermal analysis presented in Section 6.2 the maximum temperature of the first wall could be 20 °C higher, at 778 °C, which would entail a loss of about 20 MPa in the yield stress of the material. It is quite likely that a less conservative rule of the code can accommodate such an increase in temperature.

9. Fabrication

The AFS that we selected is an ODS ferritic alloy. One of the difficulties with ODS ferritic steel is fabrication. Because this AFS structural material is new, and still being developed, the joining method it is not altogether resolved. Thus far, the only joining method that seems to work is diffusion bonding or hipping. In this process, surfaces are abutted together under pressure and high temperature for a period of time. In this way, the surfaces are diffused together. Conventional welding techniques, such as gas tungsten arc (TIG), gas metal arc (MIG), laser or plasma welding have not been successful due to the presence in the material of small quantities of ceramic particles. Research is presently ongoing, and it is possible that these difficulties will be overcome. Another limitation in the use of ODS steel is in forming. When a sheet of steel is formed into a certain shape by stretching, care must be taken to insure that the amount of extension is relatively uniform in all directions. That is required to insure uniformity of strength in all directions. Thus, in fabricating the FW and blanket, forming and diffusion bonding are the primary techniques used. In some cases, several diffusion bonding steps are necessary to build the blanket.

As can be seen from the figures in this paper, the blanket is fairly complicated, consisting of an FW assembly attached to a blanket assembly immediately behind it. The FW assembly has channels going in the poloidal direction for cooling the FW surface heat incident on it. Furthermore, these channels enclose another set of tubes, which contain lead (Pb) used as a neutron multiplier. The rear part of the blanket is divided into three parts; side channels and back channels, which are situated along the perimeter of the segments, and a large central channel in the middle as shown in Fig. 1.

For our study, we have limited ourselves to diffusion bonding as the only means of fabricating the blanket. Two methods of fabrication have been considered, both using preliminary welding in preparation to diffusion bonding. In the first method, the back plate, with the Pb channels already attached, is welded in one piece around its perimeter. In the second method, a strip of plate with the Pb tube attached is welded to each individual channel first. Then the FW channels are lined up in the toroidal direction and diffusion bonded to a back plate. Detailed discussion of these proposed methods are presented in reference [6], which is an accompanying paper in this issue.

Assembling these segments using diffusion bonding stretches the present technology of this process. However, it is hoped, that with additional research and development, it will become possible.

10. Tritium handling, FLiBe handling and safety

In this section we explore some of the safety issues associated with the re-circulating blanket design. In particular, we examine the site boundary dose during a worst-case (frequency $< 10^{-6}$ per year) confinement-boundary-bypass accident. A confinement-bypass accident was chosen because, based on a previous safety study [30], this accident can produce significant environmental releases. The worst-case confinement-bypass accident examined here is one that is postulated to occur as a result of a total loss-of-site-power, which leads to a loss of plasma control and an induced plasma disruption. The electromagnetic currents generated in the internal components of the vacuum vessel (VV) by this disruption produces forces that in theory fail the windows of a diagnostic port or plasma-heating duct.
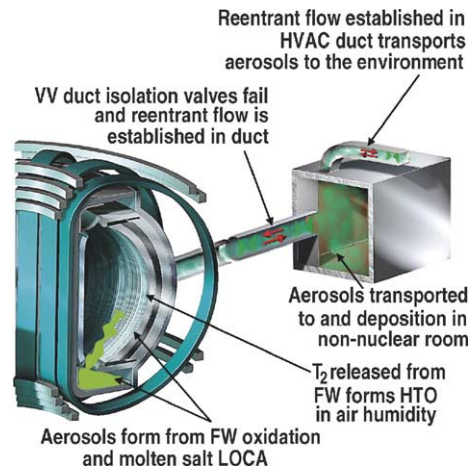
Fig. 24. Schematic of confinement bypass-accident scenario, illustrating mobilization and transport mechanisms.

In addition, the postulated rapid plasma current decay of this disruption produces runaway electrons, when lost from the plasma confinement field, fail the FW by melting. As a consequence, air from a room adjoining the reactor enters the plasma chamber by way of the failed VV port. This air reacts with the hot metal and spilt molten salt inside of the VV to mobilize radioactive material, and to transport this mobilized material into the adjoining room by natural convection airflow through the failed VV port. Fig. 24 contains a schematic of the envisioned failed VV configuration and mobilization/transport mechanism of this event. Because the adjoining room is a 'non-nuclear' room, that is a room that requires frequent human access for equipment maintenance and would not be leak tight, natural convection airflow to the environment can develop in a duct of the heating-ventilation-air conditioning (HVAC) system of this room. Of ultimate concern regarding this accident is the risk this accident poses to the public. Under the DOE Fusion Safety Standard [31], the maximum allowed dose at the site should not exceed 10 mSv during worst-case weather conditions [32]. This dose limit ensures that a site evacuation plan will not be required for a facility that adopts this blanket design concept.

10.1. Tritium inventories

The major radiological inventories in this blanket design are the activation products in the AFS struc-

tures, the activation products in the FLiBe coolant, and the tritium in blanket and cooling system components. These inventories can be mobilized during this accident scenario by AFS oxidation or coolant evaporation in the case of activation products, and by permeation in the case of tritium. The radioactive inventories of the AFS structures and the FLiBe salt were discussed in Section 4. In this section we present the predicted tritium inventory associated with this design concept.

Tritium permeation and inventories in this blanket design are radiological safety concerns during both normal operation and accident conditions because the tritium solubility and permeability in the FLiBe are very low while in contrast the tritium solubility and permeability in the AFS are very high. Because the tritium bred in the FLiBe readily permeates through pipe walls into the halo heating system of the primary heat transport system (PHTS) [7] and into the secondary Brayton power cycle system through the primary heat exchanger tube walls, the tritium control strategy adopted for this blanket concept is to use the helium cleanup system to recover this tritium. In addition, the cool outer walls of the PHTS pipes and Brayton cycle pressure boundary ($\sim$90 °C) help to reduce permeation from the primary and secondary heat transport systems into the atmosphere of confinement building rooms that contain these systems. The tritium cleanup system being considered in this design is that being proposed by reference [33] as a helium coolant purification system (CPS) for the European solid breeder blanket design concept. This purification system removes 0.1% of the helium flow as a 'slip stream' for removal of hydrogen isotopes that enter the helium coolant by permeation. The removal efficiency of this purification system is reported to be 95%.

As described in detail by reference [34], we used the Tritium Migration Analysis Program (TMAP) [35] to predict tritium permeation and inventories for this blanket concept. Two sources of tritium were considered: (1) tritium ions that escape the plasma magnetic field and impinge on the AFS FW, and (2) tritium that is bred within the FLiBe coolant. Based on information presented in reference [36], we estimate that an average FW implantation flux of tritium ions is 2.1×10^{20} ions/m^2 s. The rate at which tritium must be bred within the FLiBe should be slightly larger than the rate at which tritium is consumed by the plasma fusion reaction. This rate is 152 g/day per 1000 MW

of fusion power produced by the plasma. The TMAP model developed for this blanket concept includes representations of the major reactor components for both the primary and secondary heat transport systems. The primary system components are the blankets, high temperature shields (HTS), mixer, triple walled piping, and heat exchanger. The FLiBe or halo helium flow within these components was also modeled, including the halo helium cleanup system. The Brayton cycle secondary system components are the pressure boundary wall, cooler tube walls, and secondary helium cleanup system.

The predicted inventory of tritium in the AFS steel of the primary loop is about 82 g. Nearly 75% of the 82 g inventory resides in the in-vessel components, with 40 g in the primary blanket and 21.5 g in the secondary blanket. Because of the low solubility of hydrogen isotopes in FLiBe and the helium cleanup system efficiency, the predicted tritium inventories in the primary loop FLiBe and secondary loop helium are only 1.1 and 5.5 g, respectively. Of the 511 g/day bred in the blankets, 48.5 g/day permeates through the FW into the vacuum vessel (VV), 4.5 g/day permeates through the back wall of the HTS into the vacuum vessel, 382.3 g/day permeates through the heat exchanger into the secondary system, and 75.7 g/day permeates through piping into the halo heating system.

The allowed public dose from routine airborne radionuclide releases is 10 mrem/year (0.1 mSv/year) [37]. For a stacked release of tritium under worst-case weather conditions this allowable dose translates into a tritium mass release limit of 1.3 g/year. Tritium permeation from the primary piping/mixer walls and the secondary pressure boundary is predicted to be about 1.2 g/year. This is within the limit if the HVAC system exhaust flow is stacked. However, to meet the Fusion Safety Standard goal that all doses should be kept "as low as reasonably achievable" an air detritiation system will likely be required to accommodate the possibilities of ground level releases and leaks from the heat transport systems through valves, pumps, etc.

The allowed public dose from routine release of tritium into community drinking water is 4 mrem/year (0.4 mSv/year), which translates into a concentration of 20,000 pCi/l [38]. Because the tube walls of the coolers in the secondary Brayton cycle would be constructed of aluminum, the permeation rate into the cooling water at a temperature of 55 °C would only be 11 mCi/day.

Given the water flow rate through these coolers, this translates into an increase of 13 pCi/l per pass through the cooler, which is below the drinking water limit. However, this water will not be released directly into the environment, to guard against the possibility of leaks.

10.2. Hazard assessment

Given the radiological inventories and decay heating presented by previous sections of this paper, we can now analyze the thermal response of the re-circulating blanket design during accident conditions, and based on the predicted response of this design estimate the consequence of this confinement bypass accident on public safety.

10.2.1. Thermal-hydraulic response

We use the MELCOR code [39–41] to analyze the consequences of this confinement bypass accident for the re-circulating blanket design. The input models for this blanket design include a complete one dimensional radial conduction/thermal-radiation heat transfer model of the in-vessel components and an entire PHTS. The conduction model includes the FW, HTS, and VV walls. The PHTS model includes the pumps, valves, mixers, piping, accumulator, and heat exchanger of this system. This model represents one quadrant of the reactor. In addition, the input models that were developed include (1) the free volume within the VV, (2) the confinement building non-nuclear room and HVAC system duct, and (3) a duct that connects the VV to the non-nuclear room.

As determined by previous design studies [42,43], a very reliable method for removing decay heat from a reactor is by the passive means of natural convection within the VV cooling system. The International Thermonuclear Experimental Reactor (ITER) project has designed the ITER-FEAT VV water-cooling system to provide 1.6 MW natural convection cooling during off-normal events [44]. We have adopted these same system characteristics for the VV of our MELCOR model.

Because the PHTS exists as four separate loops, that is as quadrants, this bypass accident will result in one quarter of the in-vessel components experiencing a loss-of-cooling accident (LOCA) through the failed FW, while the remaining three quarters of the components experience a loss-of-flow accident (LOFA) as
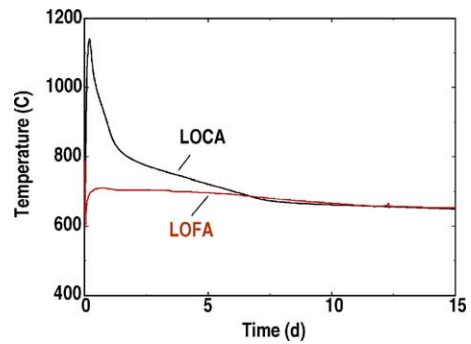
Fig. 25. Thermal response of the APEX solid FW FLiBe-cooled blanket during LOCA and LOFA conditions.

pump power is lost. Fig. 25 contains FW temperatures for the re-circulating blanket during a LOCA and a LOFA. During the first 1000 s of the LOCA the FW temperature will drop from an average of 760 to near 650 °C as a result of FLiBe cooling during the LOCA. After the FLiBe completely drains from the loop, a condition that takes about 500 s to develop, the FW temperature reaches a maximum value of 1140 °C in 5 h. This temperature rise is nearly adiabatic, and this temperature history only reverses direction once the decay heat decreases to a level that matches the radial loss to cooler internal reactor components, such as the VV. The FW temperatures during a LOFA are markedly different than those of a LOCA. Initially the FW cools from the circulation of the FLiBe without reactor power, then the FW temperature returns to near its initial value in 5 h at a temperature of about 710 °C. It is clear from comparing the LOCA and LOFA results that FLiBe plays an important safety role in maintaining low in-vessel component temperatures during accident or routine maintenance conditions and should not be drained from the system without at least a 5-day waiting period.

10.2.2. Radioactive material mobilization

The primary way that the AFS activation inventories could be mobilized is by oxidation as the ingress air brings oxygen into contact with the high temperature FW. Oxidation data for the AFS steel being proposed for this blanket does not exist. However, oxidation data for a low-activation-ferritic steel alloy (HT-9) has been experimentally obtained by reference [45]. Based on this data and the FW temperatures predicted during this

confinement bypass accident, the mass of AFS oxides mobilized during the first week of this accident will be about 105 kg.

Mobilization of the tritium inventories will occur as a result of permeation of this tritium from various AFS steel structures within the PHTS into the FLiBe coolant where it is carried to the FW and there permeates through the FW and into the free volume within the VV. This tritium will then be converted to tritiated water (HTO) and carried by natural convection air currents to locations outside of the VV during a bypass event. We used the TMAP model described in Section 10.1 to predict the rate at which tritium is released into the VV. By the end of 1 week, 40 g has been mobilized from the re-circulating blanket design concept.

During a bypass accident, radioactive FLiBe salt components will be mobilized due to salt evaporation. Initially, this evaporation occurs in a vacuum environment, but as the air ingress proceeds this evaporation will occur at atmospheric conditions. This means that initially evaporation will occur by surface pressure alone, but because these salts are very low vapor pressure fluids, as the air density in the VV increases the evaporation will be limited by diffusion of salt molecules through a boundary layer that develops above the salt surface. Once in the VV atmosphere, these salt vapors will condense to form aerosols. We modeled both of these evaporation regimes in the MELCOR model during this accident; by assuming that salt components evaporate and condense separately, that is BeF_2 in the salt evaporates as BeF_2 and condenses to form aerosols as BeF_2. The predicted FLiBe aerosol mass from this concept reaches 100 kg within the first day. The mobilized mass reflects the temperature trends of the FW. Once the FW temperature drops below 800 °C, which occurs within 2 days, the evaporation rate becomes very low.

10.2.3. Radioactive material release and resulting site boundary doses

The quantity of mass released from the re-circulating blanket design concept to the environment by way of the non-nuclear room ventilation system for all three radioactive inventories appears as a function of time in Fig. 26. By the end of 1 week, the masses released are 695 g of FLiBe, 35 g of AFS oxides, and 5.7 g of tritium. Given these results and the activation inventory of Section 4, the dose at the site boundary
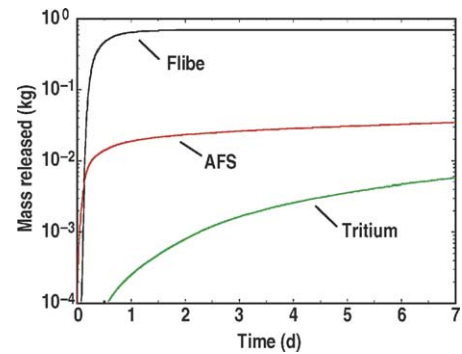
Fig. 26. Radioactive mass released to the environment from the re-circulating blanket design concept during the worst-case confinement-bypass accident.

can be estimated. From radiological dose calculations performed by reference [46], the dose for stacked releases of tritium as HTO is 77 mSv/kg, assuming a 1 km site boundary and worst-case weather conditions. The specific dose of FLiBe is 0.32 mSv/kg, with 99% of the dose due to F-18. Unlike the specific dose for tritium and FLiBe, the specific dose from the AFS oxide changes with time because the oxide composition varies with temperature. The specific dose for AFS oxide is 6.7 mSv/kg at shutdown, peaks at 10.6 mSv/kg after 1 h, and drops to 5.0 mSv/kg by 7 days. The major contributors to this specific dose are Mn-54, Ca-45, and Ti-45. The dose at the site boundary is the integrated product of mass release times the specific dose. Fig. 27 contains the predicted site boundary dose for these radioactive materials. The total dose at the site boundary after 1 week, if the releases are stacked, is 0.93 mSv. This dose is well below the 10 mSv limit.
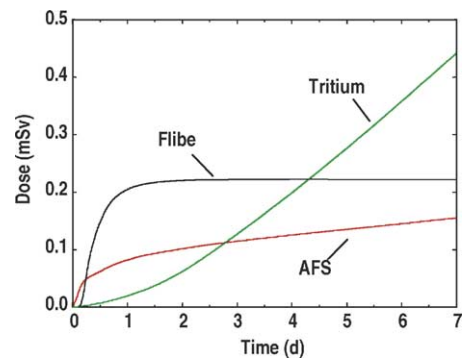
Fig. 27. Dose at the site boundary from the solid FW blanket design concept during the worst-case confinement-bypass accident.

Given the rate of release from this design concept, the facility must be isolated within an additional 4 weeks to stay below the 10 mSv limit. If these releases cannot be stacked, the facility must be isolated within 1 week to meet the limit. Even for ground releases, the time allowed for isolation and facility cleanup is adequate even for manual operation of plant remediation and isolation systems.

The remaining safety hazard that must be addressed is the radioactive inventories associated with the lead (Pb) multiplier. As noted in Section 5, Po-210 and Hg-203 are two radioactive elements that develop during neutron irradiation of Pb. These isotopes are of particular concern because their volatility in Pb makes them a dominant contributor to the dose from a Pb spill. However, because the Pb multiplier is a liquid in this blanket design, the opportunity exists for removing these isotopes during operation to levels that will ensure that the site boundary dose will not exceed 10 mSv, even if the entire Po-210 and Hg-203 inventories were to be released. This would require, if the release were to be stacked, that the Po-210 concentrations must be lowered from the equilibrium value of 30 parts-per-billion (PPB) to 0.02 PPB. Similarly, the Hg-203 concentration must be lowered from 340 to 0.3 PPB. Circulating a small amount of Pb from the multiplying zone and removing these volatile components from the Pb could accomplish this. If the removal efficiency of this system were 95% at these concentrations, the required circulation rate would be about 1100 cm^3/s, which is a complete Pb change out once every 3.3 h. To achieve the reduction in Po-210 inventory, on-line extraction of Bi (a precursor of Po-210), the process adopted by reference [47], is also proposed for this design study.

11. Conclusions and recommendations

We completed the assessment of an innovative solid first wall and blanket design that uses advanced nano-composite ferritic steel (AFS) as the structural material, Pb as the neutron multiplier and FLiBe as the tritium breeder and coolant. We selected the re-circulating flow configuration as our reference design, which allows the control of the first wall coolant heat transfer and maintains high coolant outlet temperature in spite of the use of low thermal conductivity and high viscosity molten salt FLiBe coolant. Based on the ma-

terial properties of AFS we found that the reference design can handle a maximum surface heat flux of 1 MW/m^2, and a corresponding maximum neutron wall loading of 5.4 MW/m^2. Using molten salt coolant gas cycle (MCGC) system as the power conversion system, a gross thermal efficiency of 47% can be projected. Using 4 cm of Pb neutron multiplier in front, the selected FW/blanket design has an overall tritium breeding ratio of 1.11 excluding breeding in the divertor region. Including MHD effects on the FLiBe coolant the total FW/blanket pressure drop is estimated to be 1.03 MPa. Thermal analysis results on the first wall design show that the coolant channel dimensions around the Pb channel can be adjusted to maintain coolant pressure drop at an acceptable value while designing to various materials temperature limits. Structural analysis results show that the maximum thermal stress occurs at the midplane of the blanket, and the design would satisfy the primary plus secondary stress limits including cyclic ratcheting according to the ITER structural design criteria. Safety assessment of the design shows that, with a continuous extraction of tritium from the halo helium cover gas, the design can be operated within allowable tritium release limit for both routine release and LOCA accident consitions. The facility can be operated to meet the limit of not requiring a site evacuation plan.

Main critical assumptions made in this design are the thermal, physical and mechanical properties and operating temperature range of the selected ODS ferritic steel alloy under fusion environment, and the allowable maximum interface temperatures between FLiBe/AFS and Pb/AFS.

For future development of this concept, in addition to the R&D needed to support the above critical assumptions made we will need to support the research in the following areas:

- Fabrication of ODS components and diffusion bonding will be a method to investigate.
- High temperature and neutron fluence property data for AFS for the more detailed structural analysis of the design.
- Analytical and experimental verification of the MHD effects to heat transfer and pressure drop for this design.
- Resolution on the potential concern of radiolysis effects of FLiBe under the fusion environment.

- Demonstration of the control of HF concentration, possibly through the REDOX approach.
- Demonstration on the continuous extraction of Bi in order to minimize the generation of Po-210.
- Demonstration of tritium control of the FLiBe and AFS FW/blanket and power conversion system.
- Detailed engineering design including the support of the FW/blanket structures and their response to different operational scenarios of a tokamak reactor, including normal operating and transient events such as disruption.

What we have identified is an advanced high performance AFS solid first wall and blanket design, which can be evolved from the more conventional low-activation-ferritic steel FW/blanket designs, and with the use of the low pressure and non-reactive FLiBe as the coolant and tritium breeding material. Key developmental items have been identified, and they seem to be manageable under the normal process of development for an advanced FW/blanket design that has great promise for the future development of fusion power.

Acknowledgments

References

[1] M.A. Abdou, Exploring novel high power density concepts for attractive fusion systems, Fusion Eng. Des. 45 (1999) 145–167.
[2] C.P.C. Wong, R. Nygren, C. Baxi, P. Fogarty, N. Ghoniem, H. Khater, K. McCarthy, B. Merrill, B. Nelson, E. Reis, S. Sharafat, R. Schleicher, D.K. Sze, M. Ulrickson, S. Willms, M. Youssef, S. Zinkle, Helium-cooled refractory alloys first wall and blanket evaluation, Fusion Eng. Des. 49–50 (2000) 709–717.
[3] C.P.C. Wong, L. Barleon, M. Corradini, P. Fogarty, N. Ghoniem, S. Majumdar, S. Malang, R. Mattas, K. McCarthy, B. Merrill, J. Murphy, B. Nelson, R. Nygren, M. Sawan, S. Sharafat, I. Sviatoslavsky, S. Zinkle, Evaluation of the tungsten alloy vaporizing lithium first wall and blanket concept, Fusion Technol. 39 (2001) 815–822.
[4] L. Barleon, C.P.C. Wong, The transpiration cooled first wall and blanket concept, Fusion Eng. Des. 61–62 (2002) 477–482.
[5] M. Anderson, University of Wisconsin, Personal communication, 2002.
[6] E. Sviatoslavsky, S. Mogahed, R. Majumdar, S. Mattas, P. Malang, M. Fogartym, C. Friend Wong, S. Sharafat, Solid wall recirculating blanket: geometry, materials, materials compatibility, structural evaluation, fabrication and fluid circuits, Fusion Engin. Des., this issue.
[7] B. Merrill, M. Sawan, C. Wong, L. Cadwallader, S. Malang, D.K. Sze, Safety assessment of apex advanced ferritic steel molten salt blanket design concept, Fusion Eng. Des., this issue.
[8] A. Sagara, et al., Design studies of helical-type fusion reactor FFHR, in: Proceedings of the Fourth International Symposium on Fusion Nuclear Technology, Tokyo, Japan, April 6–11, 1997.
[9] R. Moir, et al., HYLIFE-II a molten-salt inertial fusion energy power plant design-final report, Fusion Technol. 25 (1994).
[10] R.L. Klueh, et al., Microstructure and Mechanical Properties of Oxide Dispersion-Strengthened Steels, DOE/ER-0313/28, June 2000.
[11] R.L. Klueh, P.J. Maziasz, I.S. Kim, L. Heatherly, D.T. Hoelzer, N. Hashimoto, E.A. Kenik, K. Miyahara, Tensile and creep properties of an oxide dispersion-strengthened ferritic steel, J. Nucl. Mater. 307–311 (2002) 773–777.
[12] S. Ukai, M. Fujiwara, Perspective of ODS alloys application in nuclear environments, J. Nucl. Mater. 307–311 (2002) 749–757.
[13] M.S. Tillack, X.R. Wang, J. Pulsifer, S. Malang, D.K. Sze, M. Billone, I. Sviatoslavsky, Fusion power core engineering for the ARIES-ST, Fusion Eng. Des. Power Plant 65 (2003) 215–261.
[14] R. Raffray, M.S. Tillack, X. Wang, L. El-Guebaly, I. Sviatoslavsky, S. Malang, Aries-AT blanket and divertor, Fusion Technol., Part 2 39 (2) (2001) 429–433.
[15] R.E. Alcouffe, et al., DANTSYS 3.0, A Diffusion Accelerated Neutral Particle Transport Code System, LA-12969-M, Los Alamos National Laboratory, June 1995.
[16] M. Herman, H. Wienke, FENDL/MG-2.0 and FENDL/MC-2.0, The processed cross-section libraries for neutron–photon transport calculations, Report IAEA-NDS-176, International Atomic Energy Agency, March 1997.
[17] S. Malang, M.S. Tillack, et al., Development of self-cooled liquid metal breeder blankets, Forschungszentrum Karlsruhe Technical Report, FZKA 5581, November 1995.
[18] C.P.C. Wong, et al., Toroidal reactor designs as a function of aspect ratio and elongation, Nucl. Fusion 42 (2002) 547–556.
[19] P.F. Peterson, Multiple-reheat Brayton cycles for nuclear power conversion with molten salt coolants, Nucl. Technol. 144 (3) (2003) 279–288.
[20] H. Branover, Magnetohydrodynamic Flows in Ducts, Wiley, New York, 1978.
[21] S. Smolentsev, et al., Applications of the "K-epsilon" model to open channel flows in a magnetic field, Int. J. Eng. Sci. 40 (2002) 693–711.
[22] E. Blums, Yu.A. Mikhailov, R. Ozols, Heat and Mass Transfer in MHD Flows, World Scientific, Singapore, 1987.
[23] C. Chang, S. Lundgren, Duct flow in magnetohydrodynamics, Zeitschrift fur angewandte Mathematik und Physik XII (1961) 100–114.

[24] S. Smolentsev, Mathematical models for magnetohydrodynamic flows in a fusion reactor blanket, Plasma Devices Oper. 7 (3) (1999) 231–241.

[25] W.M. Kays, Convective Heat and Mass Transfer, McGraw-Hill, 1966.

[26] J.P. Holman, Heat Transfer, 8th ed., McGraw-Hill, 1997.

[27] C.P.C. Wong, B.W. McQuillan, R.W. Schleicher, E.T. Cheng, Evaluation of U.S. demo helium-cooled blanket options, in: Proceedings of the 16th IEEE/NPSS, September 30–October 5, 1995, p. 1145.

[28] ABAQUS (Version 6.3), Hibbitt, Karlsson, and Sorensen, Inc., 2002.

[29] ITER Structural Design Criteria for In-Vessel Components (ISDC), ITER IdoMS S74MA197-12-12 R0.2, 1998.

[30] R. Aymar, et al., Technical basis for the ITER final design report, Cost review and safety analysis (FDR), ITER EDA Documentation Series No. 16, International Atomic Energy Agency, Vienna, 1998, Chapter IV, pp. 36–50.

[31] DOE STD 6002-96, The safety of magnetic fusion facilities: requirements, May 1996.

[32] L. Cadwallader, D. Petti, Safety in the design of three burning plasma experiments, in: Presented at the 15th Topical Meeting on the Technology of Fusion Energy, Washington, DC, November 17–21, 2002. Fusion Sci. Technol. 44 (2) (2003) 382–387.

[33] L. Berardinucci, M. Dalle Donne, Tritium control in the European helium cooled pebble breed blanket, J. Fusion Technol. 2 (1997) 1427.

[34] R. Nygren, et al., A CLIFF design based on flinabe and advanced ferritic steel, Fusion Eng. Des., this issue.

[35] B.J. Merrill, J.L. Jones, D.F. Holland, TMAP/MOD1: Tritium Migration Analysis Program Code Description and User's Manual, Idaho National Engineering Laboratory Report, EGG-EP-7407, April 1988.

[36] O.V. Ogorodnikiva, et al., Tritium permeation through the first wall of the EU-HCPB blanket, Fusion Eng. Des. 49–50 (2000) 921.

[37] U.S. Code of Federal Regulations, Title 40, Protection of the Environment, Part 61, National Emission Standards for Hazardous Air Pollutants, Subpart H, National Emission Standards for Emissions of Radionuclides other than Radon from Department of Energy Facilities, Section 92, Standard, U.S. Government Printing Office, Washington, DC, November 13, 2002.

[38] U.S. Code of Federal Regulations, Title 40, Protection of the Environment, Part 141, National Primary Drinking Water Regulations, Subpart B, Maximum Contaminant Levels, Section 16, Maximum Contaminant Levels for Beta Particle and Photon Radioactivity from Man-made Radionuclides in Community Water Systems, U.S. Government Printing Office, Washington, DC, November 26, 2002.

[39] R.O. Gauntt, et al., MELCOR Computer Code Reference Manuals: Version 1.8.4, NUREG/CR-6619, Vol. 2, Rev. 1, July 1997, HS-RM 37-41.

[40] B.J. Merrill, R.L. Moore, S.T. Polkinghorne, D.A. Petti, Modifications to the MELCOR Code for application in fusion accident analysis, Fusion Eng. Des. 51–52 (2000) 555–563.

[41] R.L. Moore, FLiBe thermal properties for use with the fusion safety multi-fluid equation of state package, Idaho National Engineering and Environmental Laboratory Report, INEEL/EXT-2000-00670, May 2000.

[42] R. Aymar, et al., Technical basis for the ITER final design report, Cost reviews and safety analysis (FDR), ITER Design Team Document, S CA LS 3997-12-19 F1, December 1997, pp. 4.3–5.

[43] C.P.C. Wong, et al., Evaluation of the tungsten alloy vaporizing lithium first wall and blanket concept, Fusion Technol. 39 (2001) 815–822.

[44] R. Aymar, et al., ITER-FEAT plant description document, ITER Design Team Document, G A0 FDR 101-07-13 R1.0, July 2001, Chapter 2.2, p. 9.

[45] K.A. McCarthy, G.R. Smolik, S.L. Harms, A summary and assessment of oxidation driven volatility experiments at the INEL and their application to fusion reactor safety assessments, Idaho National Engineering and Environmental Laboratory Report, EGG-FSP-11193, September 1994.

[46] M. Abbott, Revised results – MACCS2 doses for fusion isotopes released to the atmosphere using P-G dispersion parameters, An INEEL letter to D.A. Petti, MLA-11-99, April 14, 1999.

[47] S. Malang, T. Mattas, Comparison of lithium and eutectic lead–lithium alloy, two candidate liquid metal breeder materials of self-cooled blankets, Fusion Eng. Des. 27 (1995) 399–406.